Electronic Supplementary Material (ESI) for Nanoscale.

Supplementary material

Uncertainty Quantification of a DNA Origami Mechanism Using a Coarse-Grained Model and Kinematic Variance Analysis

Chao-Min Huang[1], Anjelica Kucinic[2], Jenny V. Le[3], Carlos E. Castro[1, 3] and Hai-Jun Su[1*]*

[1]Department of Mechanical and Aerospace Engineering, [2]Department of Chemical and Biomolecular Engineering and [3]Biophysics Graduate Program, The Ohio State University, Columbus, Ohio 43210, USA

Table of Content:

1. cadnano routing and CanDo result

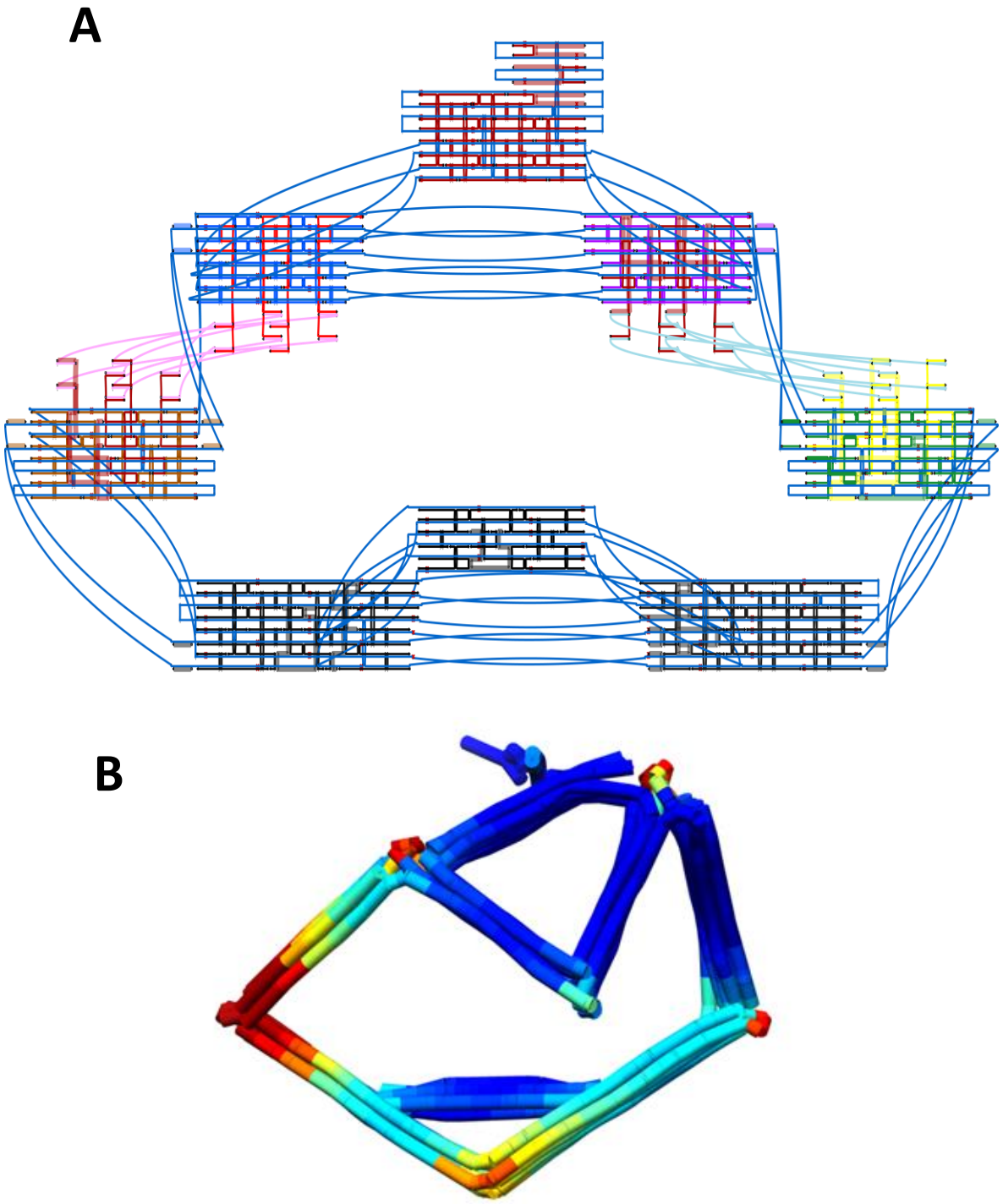

Figure S1: (A) cadnano design diagram[1] of the SLL with overhangs for actuation included. (B) CanDo[2,3] result of the SLL design.

2. Rigid body transformation (RBT) for “Virtual Assembly” of DOM designs.

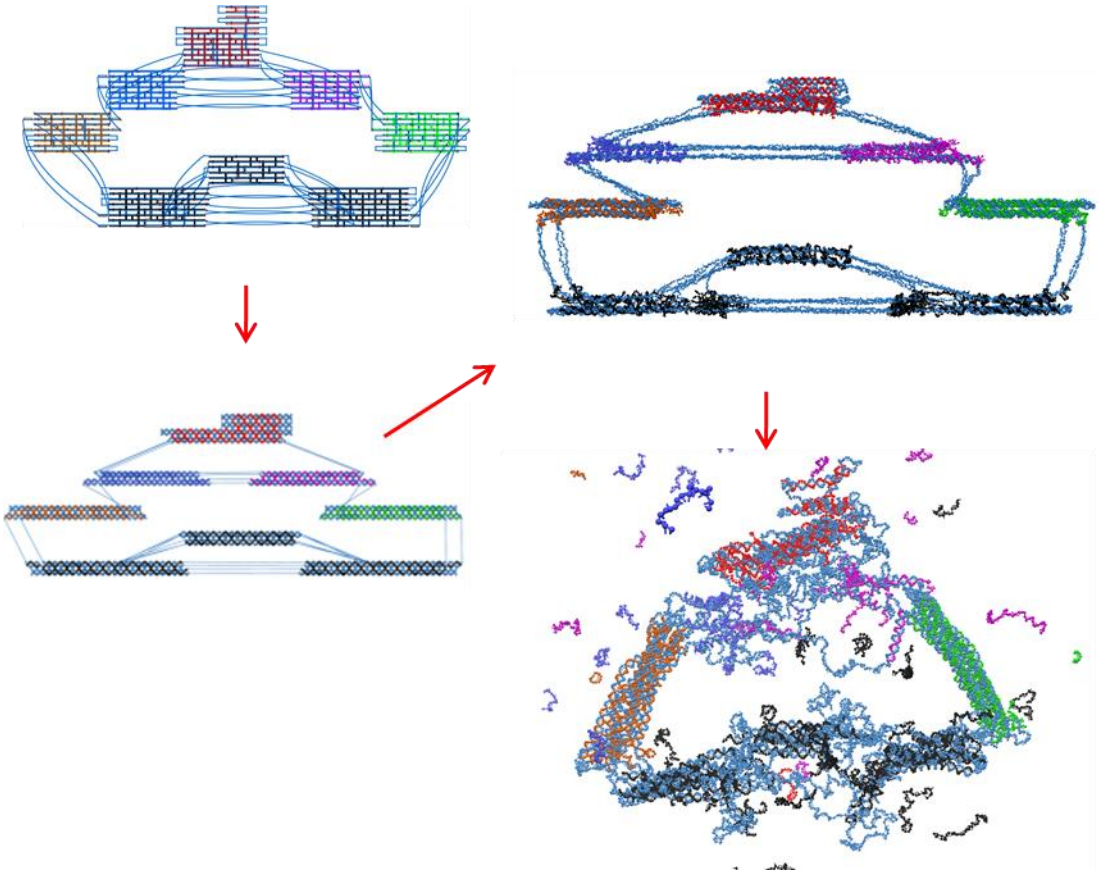

Figure S2: Directly translating the cadnano design into an oxDNA simulation without RBT yields unsuccessful relaxation. The relaxation step aims to equalize the bond distances between neighboring bases within certain range. When performing the relaxation step, a portion of staples dissociated from the scaffold strand likely due to the initial configuration being far from a physically realistic assembly.

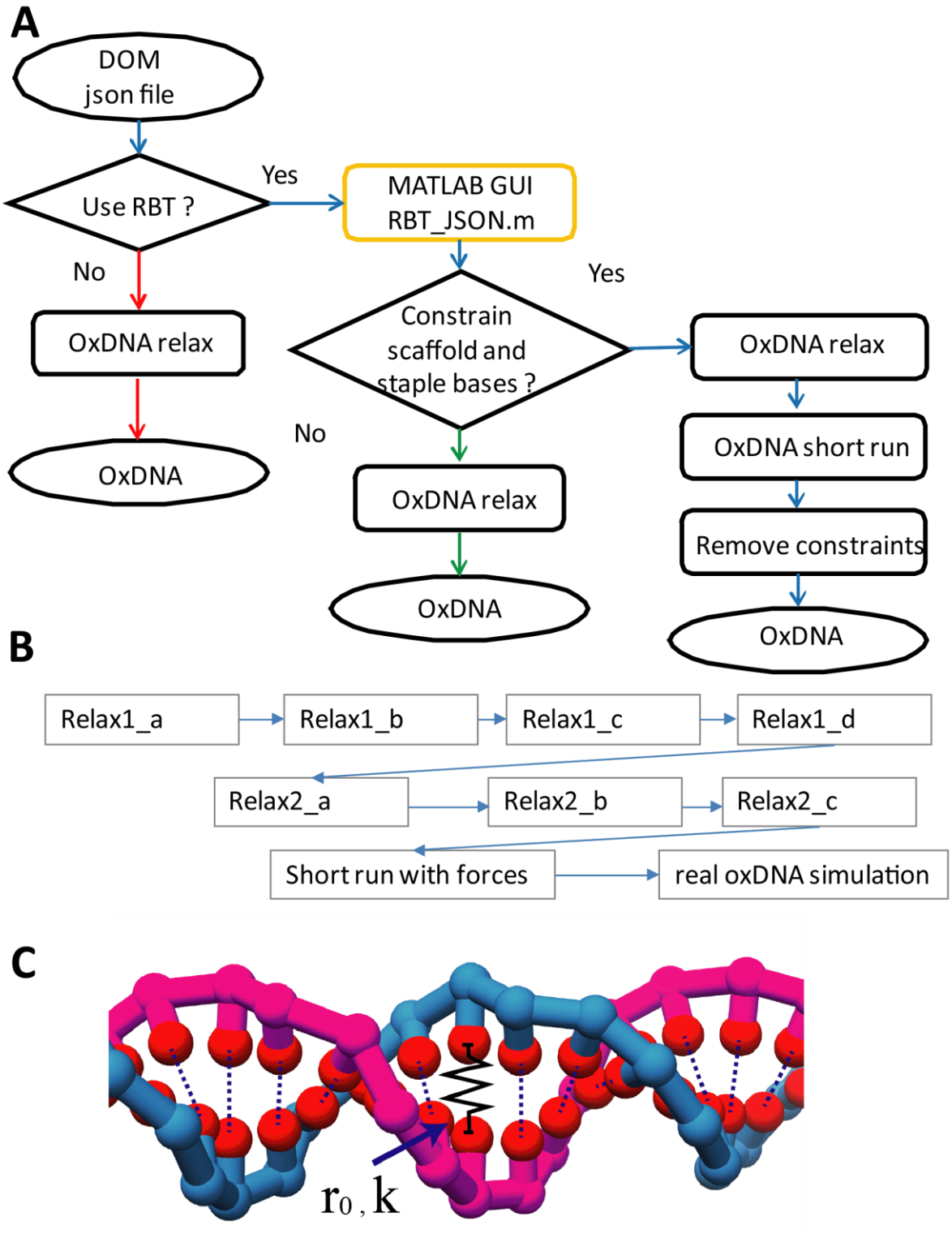

Figure S3: Flowchart of simulation processes with and without virtual assembly using RBT. (A) Typical molecular dynamic (MD) simulations[4] involve converting data formats, relaxing designed

structures, and simulating a relaxed configuration. The red path is the direct process of relaxing the configuration from the design without virtual assembly, visualized in Figure S2. The green path is the process of applying RBT without constraining scaffold and staple bases, visualized in Figure S6. The blue path that includes the virtual assembly step and constraining scaffold/staple bases was our primary workflow with results visualized in Figure 2. (B) Details for the relaxation step. After RBT, original forced connections in cadnano still remain over-stretched but close to correct assembly orientations. To adjust neighboring bonds into the FENE potential curve, the relaxation step composed of oxDNA1 (input files: Relax1_a, Relax1_b, Relax1_c, and Relax1_d) and oxDNA2 (input files: Relax2_a, Relax2_b, and Relax2_c) model is required. In the relaxation step, the neighboring bonds on backbone are substituted to unrealistic linear springs. It is possible for the bases on both sides of the forced connections to move too much and cause the numerical instability of the system. To avoid that, the spring constants and the time step are gradually increased as listed in Table S1. The second half of the relaxation uses the oxDNA2 model, which introduces the major and minor groove[5]. In addition, for large systems like DNA origami, the oxDNA2 model also tunes the global twist to correct parameters[5]. After the relaxation step (Figure 2D), the neighboring bonds are within FENE potential curve but the center locations of each bundle still slightly separated. Thus, a very short simulation (input file: short_run) with mutual forces was applied to bring all bundles together (Figure 2E). Finally, the oxDNA simulations were performed with at different time scales and different initial configurations to observe the thermal fluctuation. Note that the mutual forces were used in the entire relaxation step. (C) To confirm that all staples annealed to the scaffold, the MATLAB GUI code generates a file containing thousands of "mutual trap" forces between complementary paired bases. This kind of force generates unrealistic external forces between paired bases as connected by a linear spring. The equilibrium distance r_0 is set to 1.4 nm, which is close to the minimum hydrogen bonding potential. The very high stiffness k is set to fix the relative distances throughout the entire relaxation step. Note that these forces were later removed in the real simulations present in this research.

Table S1: Selected input options for all the input files in this research. All the input files are included in the supplement .zip file.

Input files	**step**	**dt (unit: 3.03ps)**	**relax_ strength**	**Force in base-paired bases**	**Major and minor groove (oxDNA2)**	**Use GPU**
Relax1_a	1e4	2e-9	5e-7	Y	N	N
Relax1_b	1e4	2e-7	5e-2	Y	N	N
Relax1_c	1e4	5e-5	2	Y	N	N
Relax1_d	1e4	5e-3	250	Y	Y	N
Relax2_a	1e4	1e-7	250	Y	Y	N
Relax2_b	1e4	5e-5	150	Y	Y	N
Relax2_c	1e4	5e-3	150	Y	Y	N
Short_run	1e6	5e-3	N/A	Y	Y	Y
oxDNA	1e8 or 3e8	5e-3	N/A	N	Y	Y

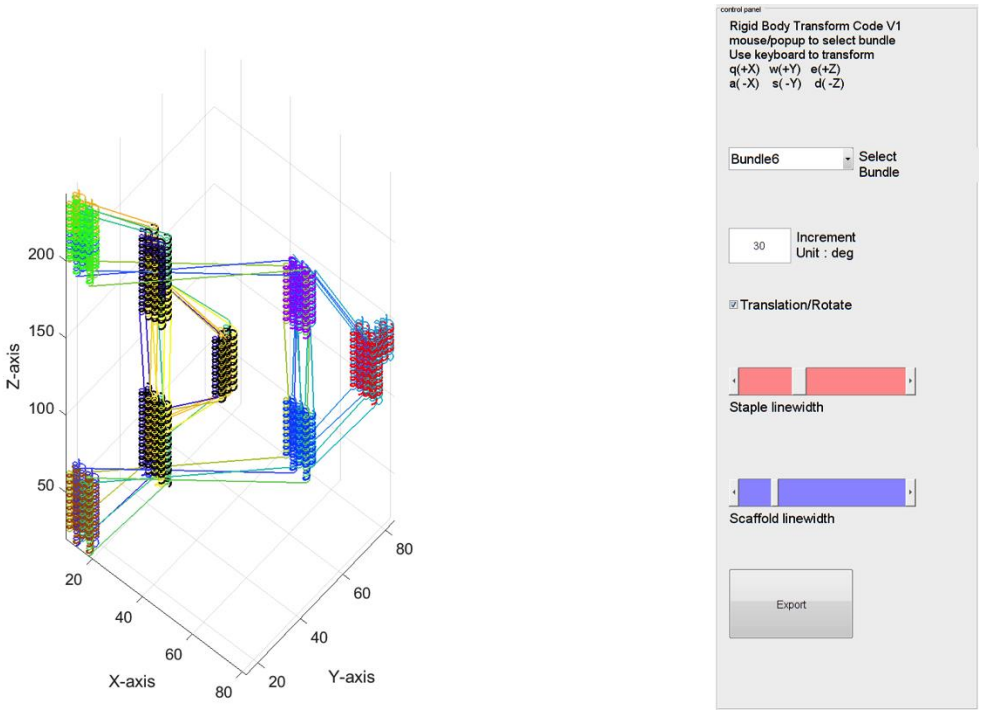

Figure S4: MATLAB graphic user interface (GUI) for virtual assembly via RBTs. This code is used to visualize the oxDNA coarse-grained model after converting cadnano json files. Users can transform each bundle by clicking/selecting a bundle, translating or rotating the bundle into approximate position for an appropriate assembled configuration.

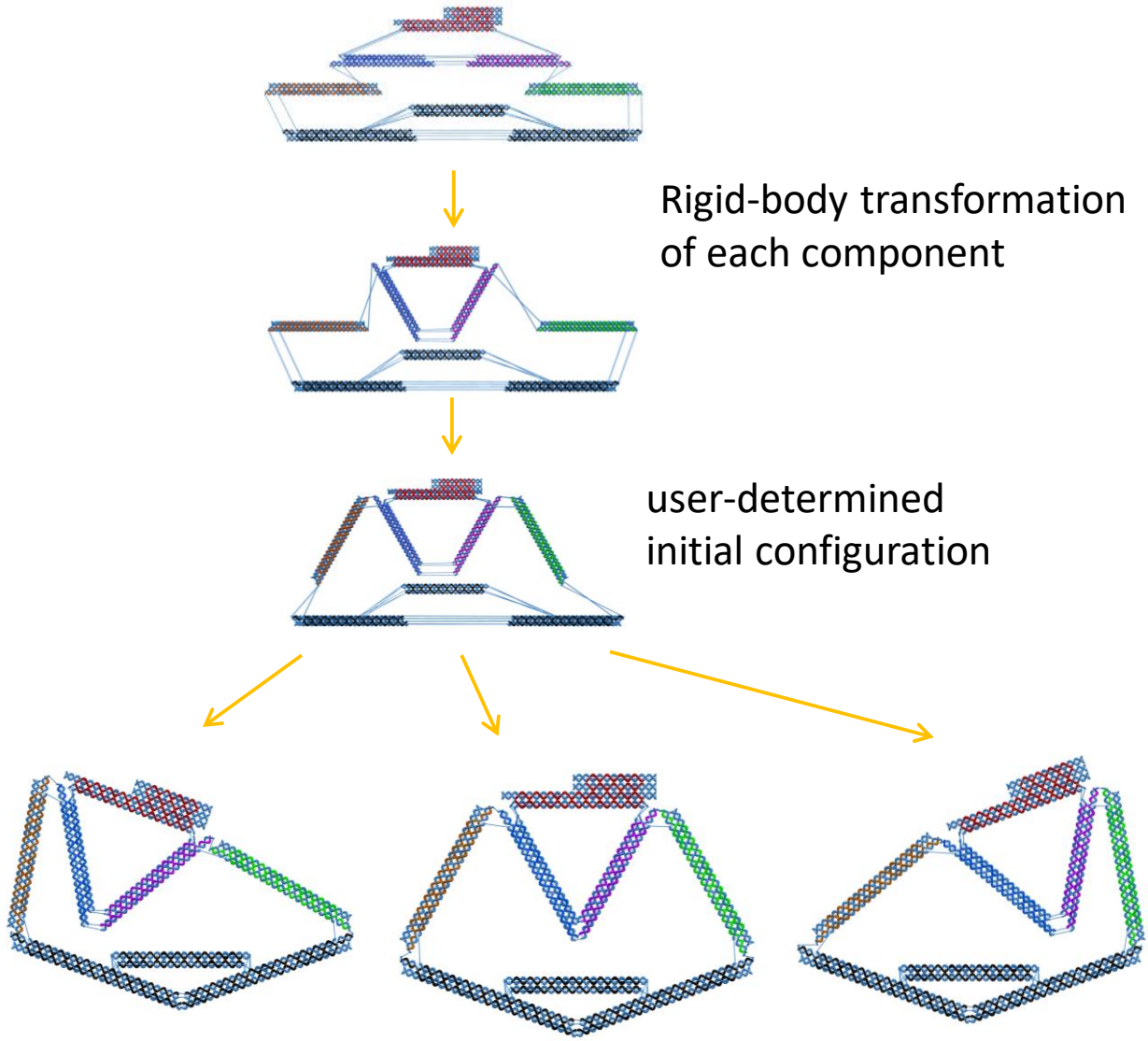

Figure S5: Intermediate steps of RBT virtual assembly. Based on the staple colors in the json files, we first categorized all bases into groups that comprise a component and each component was then applied a different RBT. By manually transforming each bundle, one can export a desired assembly with control over the initial configuration. This tremendously reduces the required relaxation time since it greatly reduces overstretched interactions. In addition, this allows us to simulate the DOM starting at various initial configurations.

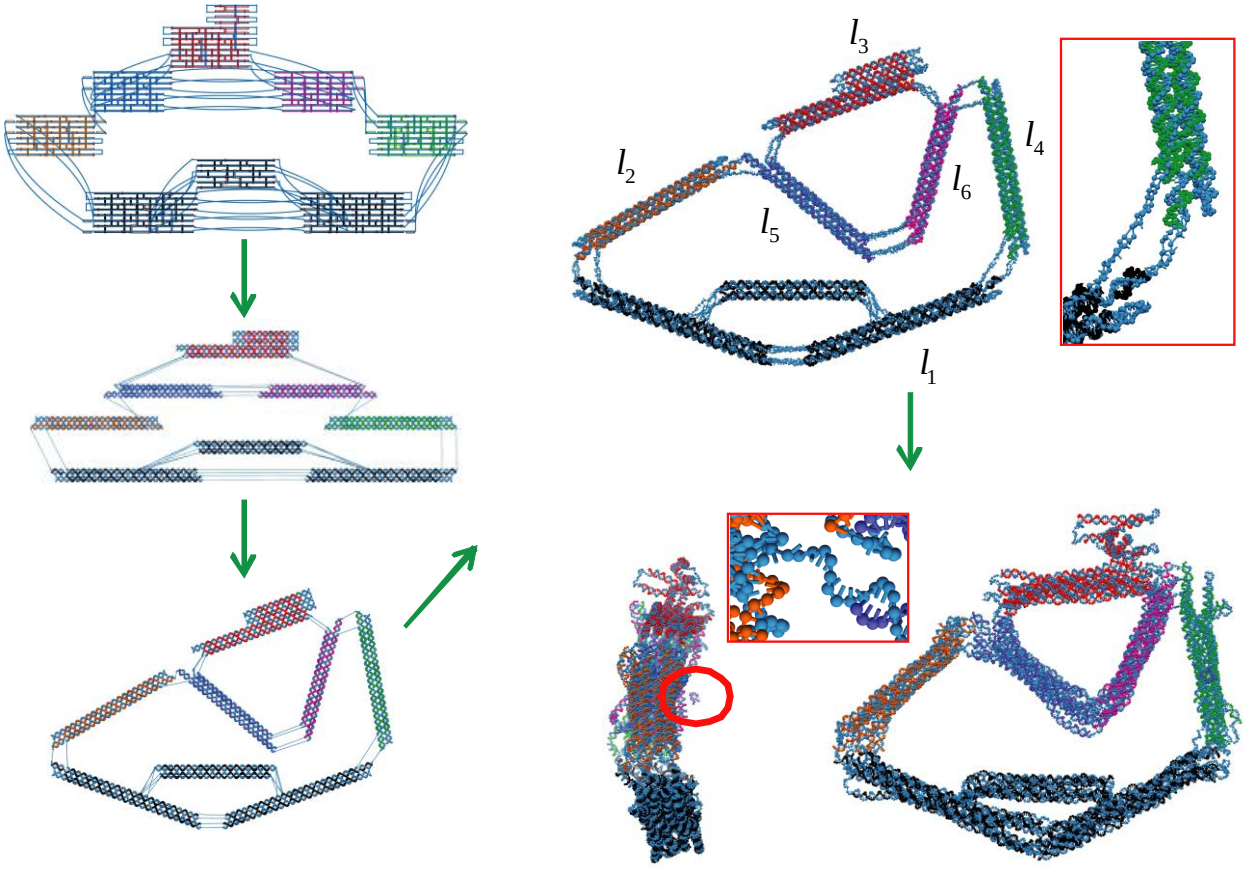

Figure S6: The oxDNA relaxation simulation with RBT but without constraining scaffold and staple bases. With the RBT, the initial configuration was almost assembled. During the relaxation step, the bases at both sides of the forced connections would move into closer proximity of each another. However, the staple bases were still in their original positions (See top-right inset). After performing the simulation, depending on the level of separation of the exported figure, some staples may dissociate from the scaffold strand (circled in red). The bottom-right inset shows the position of the staple in red circle where this staple should have bond with the scaffold.

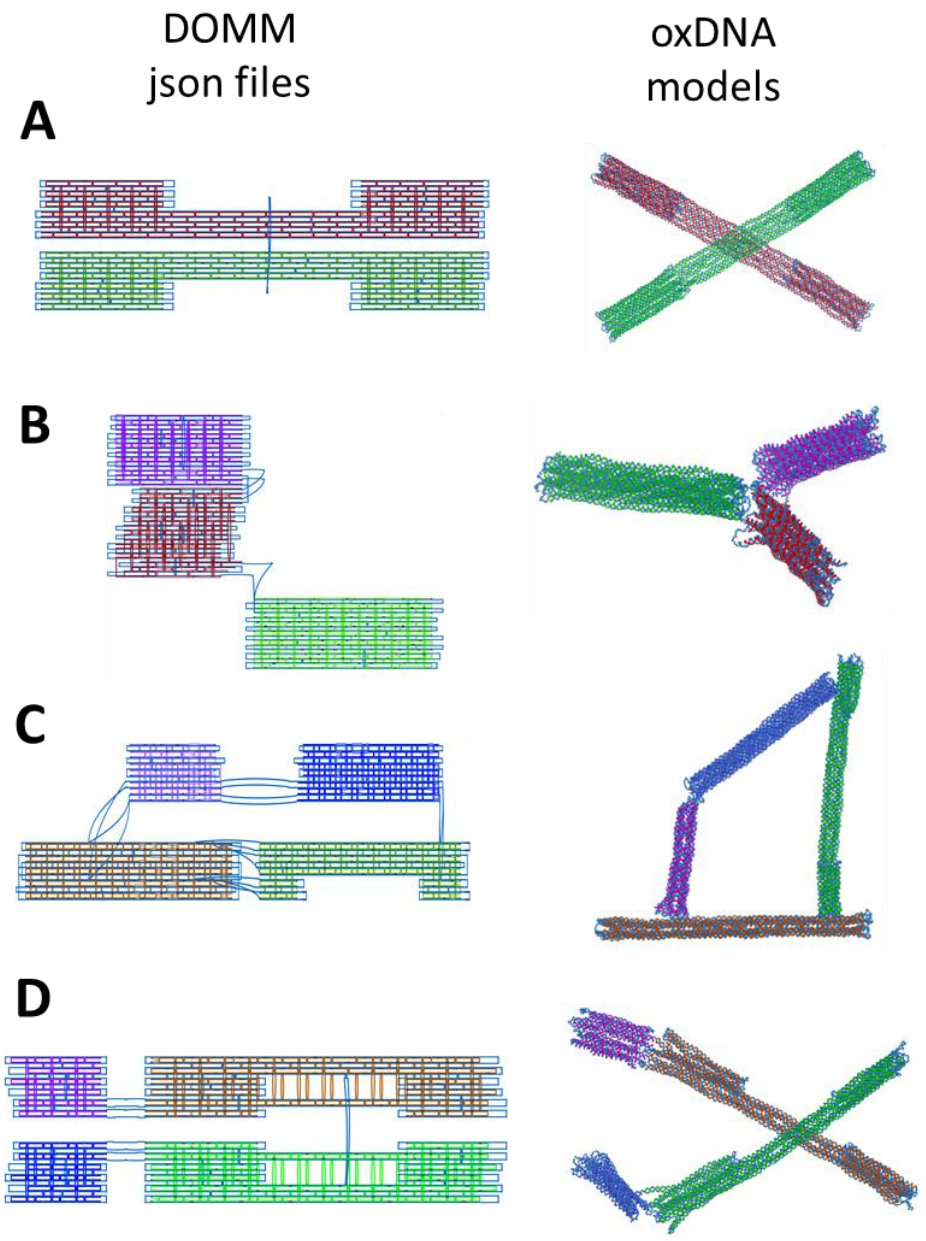

Figure S7: Additional examples of simulating DOM designs. This computational framework can be used in general multi-component dynamic structures. From top to bottom, (A) a cross-hinge, (B) a universal joint[6], (C) a bistable mechanism[7], and (D) a scissor mechanism[6] were converted to the oxDNA configurations.

3. Interpretation of the simulation results

a. The tip position

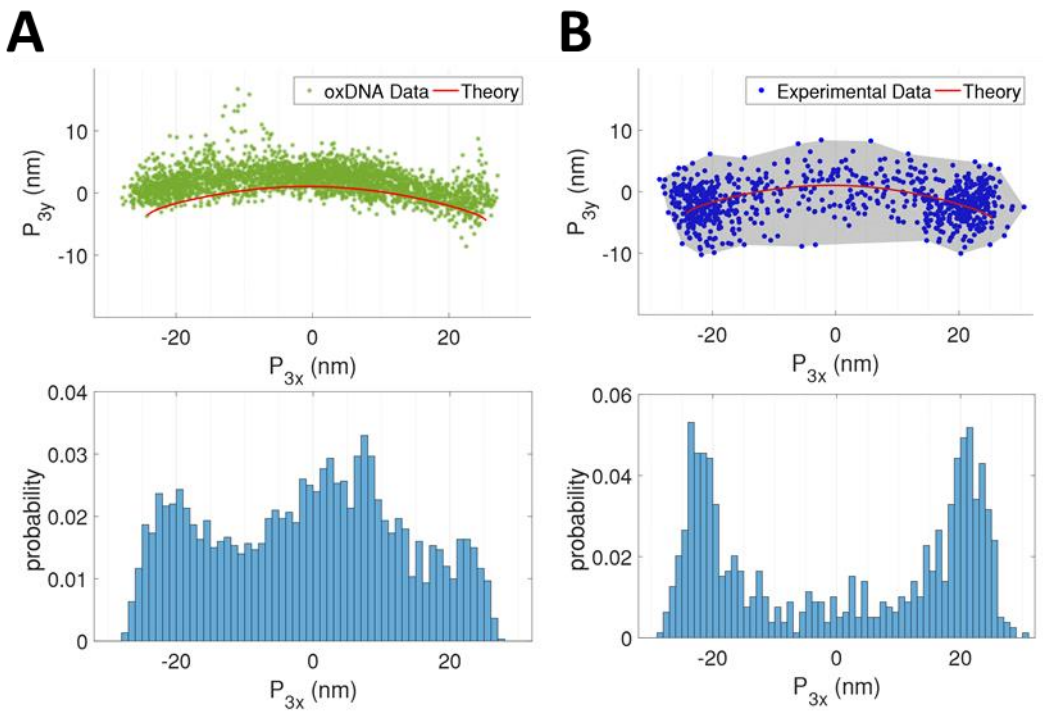

Figure S8: Comparing the probability distribution of the tip from the compiled oxDNA result with experimental data. Top row is the planar tip position P_3. Bottom row is the probability distribution along the horizontal direction. (B) The experimental data is the same as Figure 1D, which we also present here for convenience to compare with simulation results.

b. Out-of-plane motion

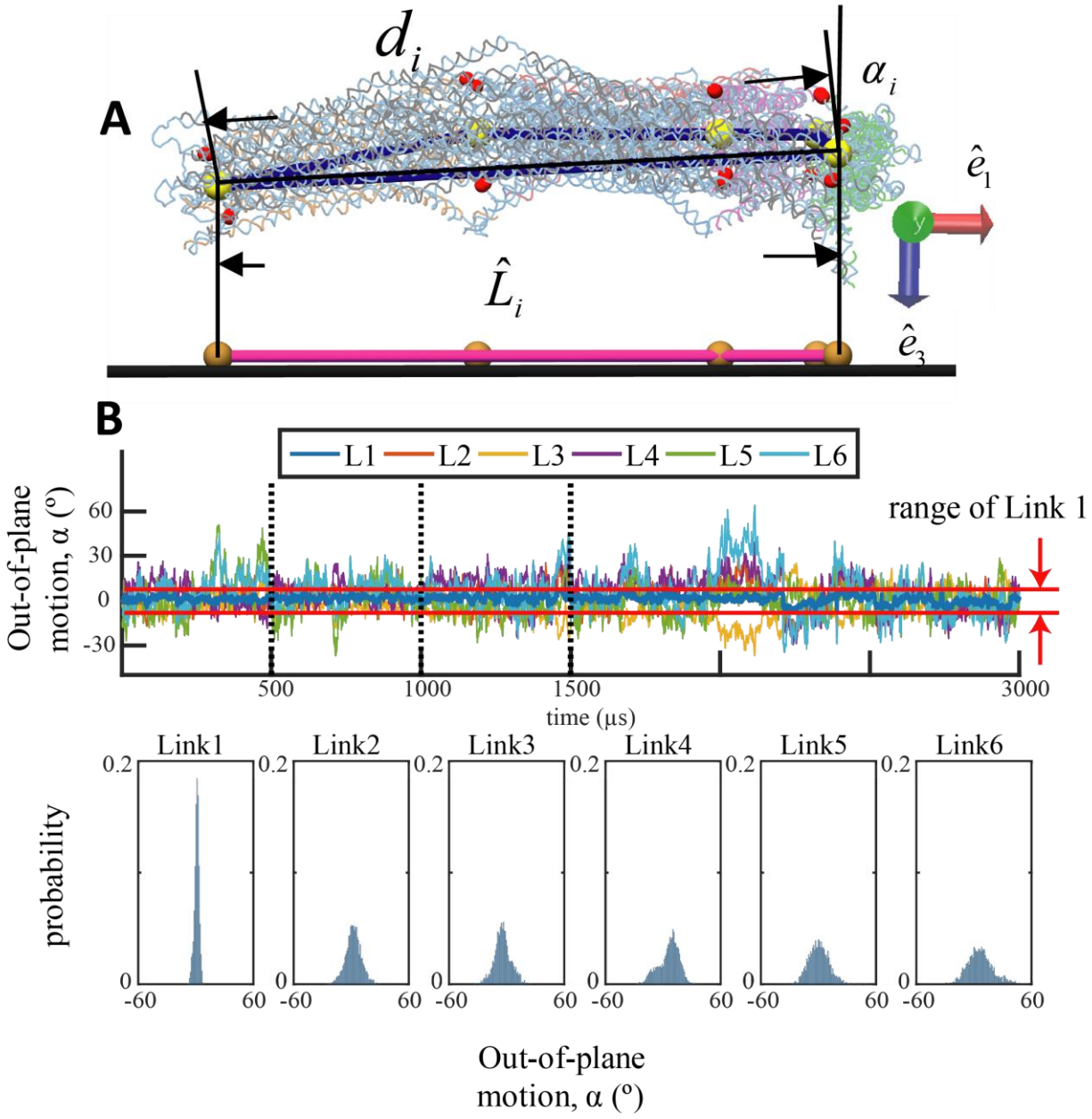

Figure S9: Schematic and the simulation data of out-of-plane motion. (A)We assumed the third eigenvector from the principle component analysis as the reference (or projection) plane. For each vertex, we determined the center of mass of the 4 nucleotides (2nt on 2 connections). The 4 nucleotides are shown as red spheres and the centers of mass are shown as yellow spheres. The links were defined as the distances between the vertex centers of mass. We calculate the angles

between links and the reference plane as out-of-plane motion. (B) We combined the four simulation results in series, separated by the dotted lines to illustrate the time-dependent fluctuation of the out-of-plane motion. The four simulations were run with different initial configurations and lengths of simulation: from left to right, starting at the center, starting at the left, starting at the right with 500μs and start at the center with 1500μs.

c. End-To-End distance

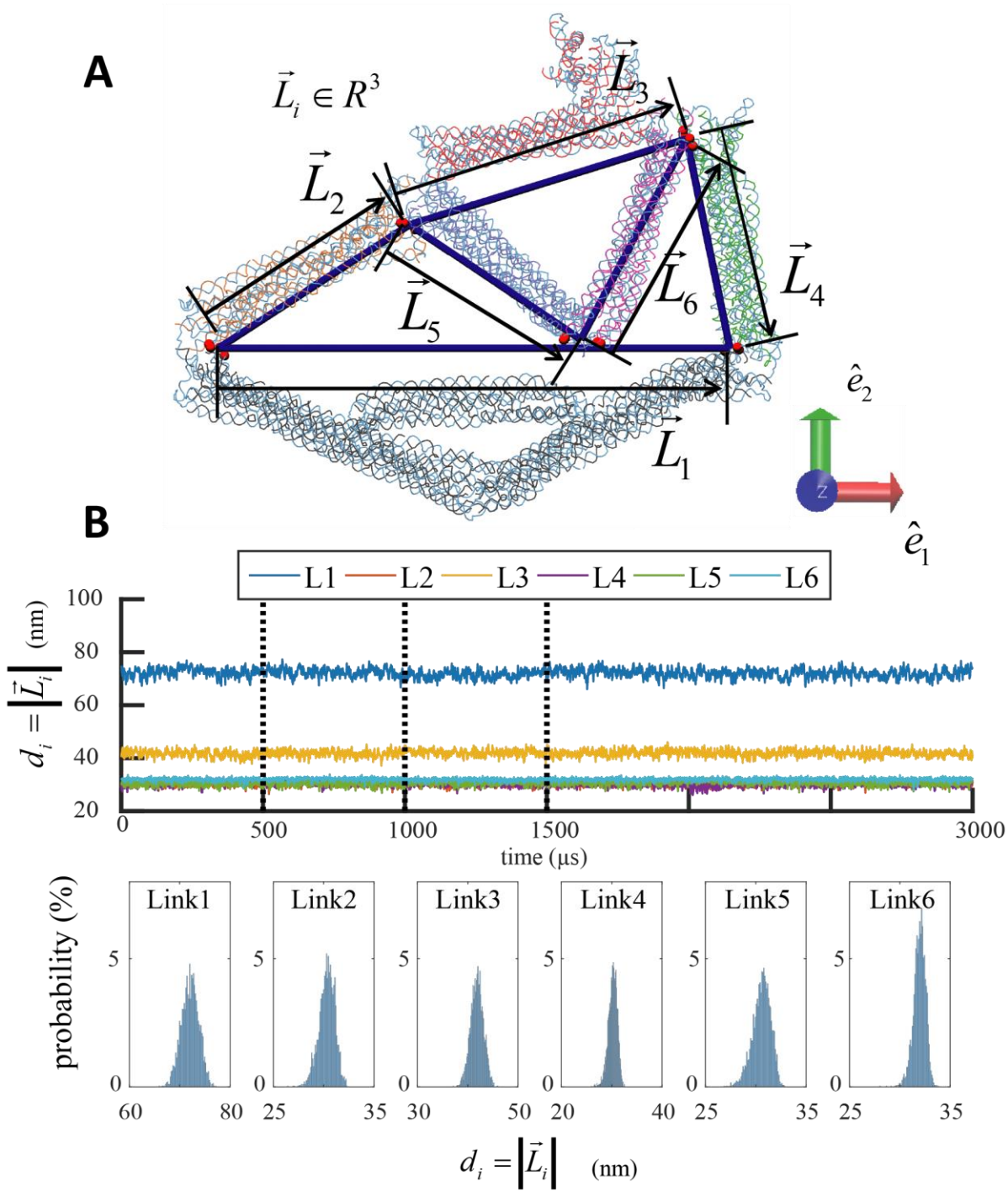

Figure S10: Schematic and the simulation data of link end-to-end distances. (A) The link lengths were tracked as the 3D vectors connecting the vertex center of mass. (B) The time-dependent

fluctuation of the end-to-end distances compiled from all four simulations. Each simulation is divided by a dashed line.

d. Correlation

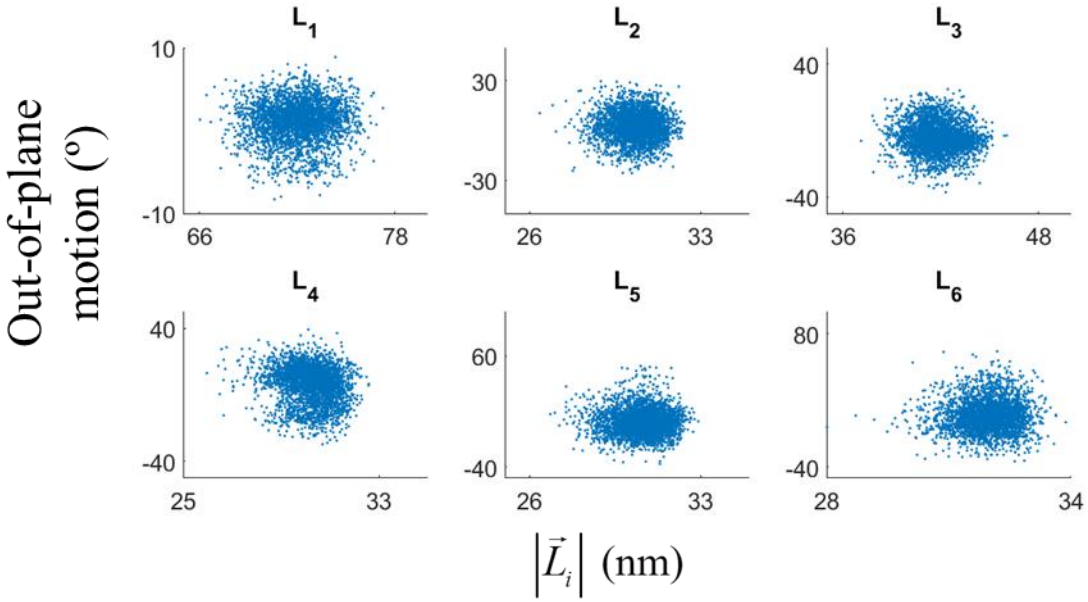

Figure S11: Correlation between out-of-plane motions and end-to-end distances for all six links. To answer if these two main error sources are related, we pulled out the data of these two errors from the trajectories to show the correlations.

e. End-to-end distances to closest cross-overs from both sides

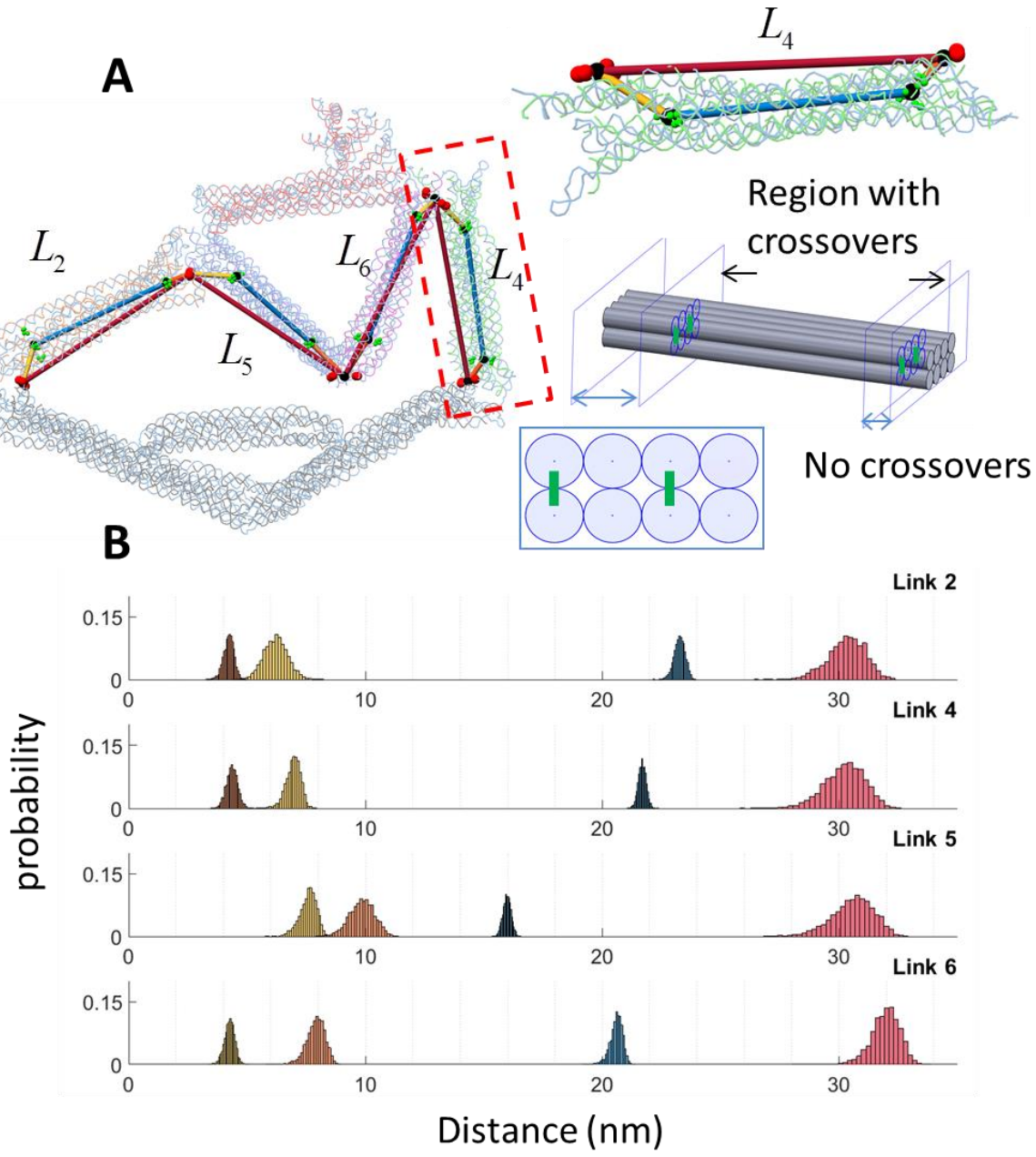

Figure S12: The flexibility of links in terms of end-to-end distances. (A) Due to the geometric constraints underlying DNA origami designs, there is often a region near the ends of links that do not contain staple cross-overs, which is likely to fray as illustrated in the SLL and link snapshots from MD simulation. We hypothesized this was the major reason for changes in end-to-end distance. To test this hypothesis, we divided the links into three regions: from the end of a link to

first set of staple cross-overs, distance between cross-overs nearest to the ends, and the distance from the nearest staple cross-over to the other end of the link. (B) We quantified the variations in length of each of these link sections for links 2, 4, 5, and 6. The length distribution of the central region between cross-overs is shown in blue, while the length distributions of the sections at the ends of the links are shown in brown and yellow. The results show that the fluctuation of the entire links (pink histograms) mainly come from the fraying on the two ends (yellow and brown).

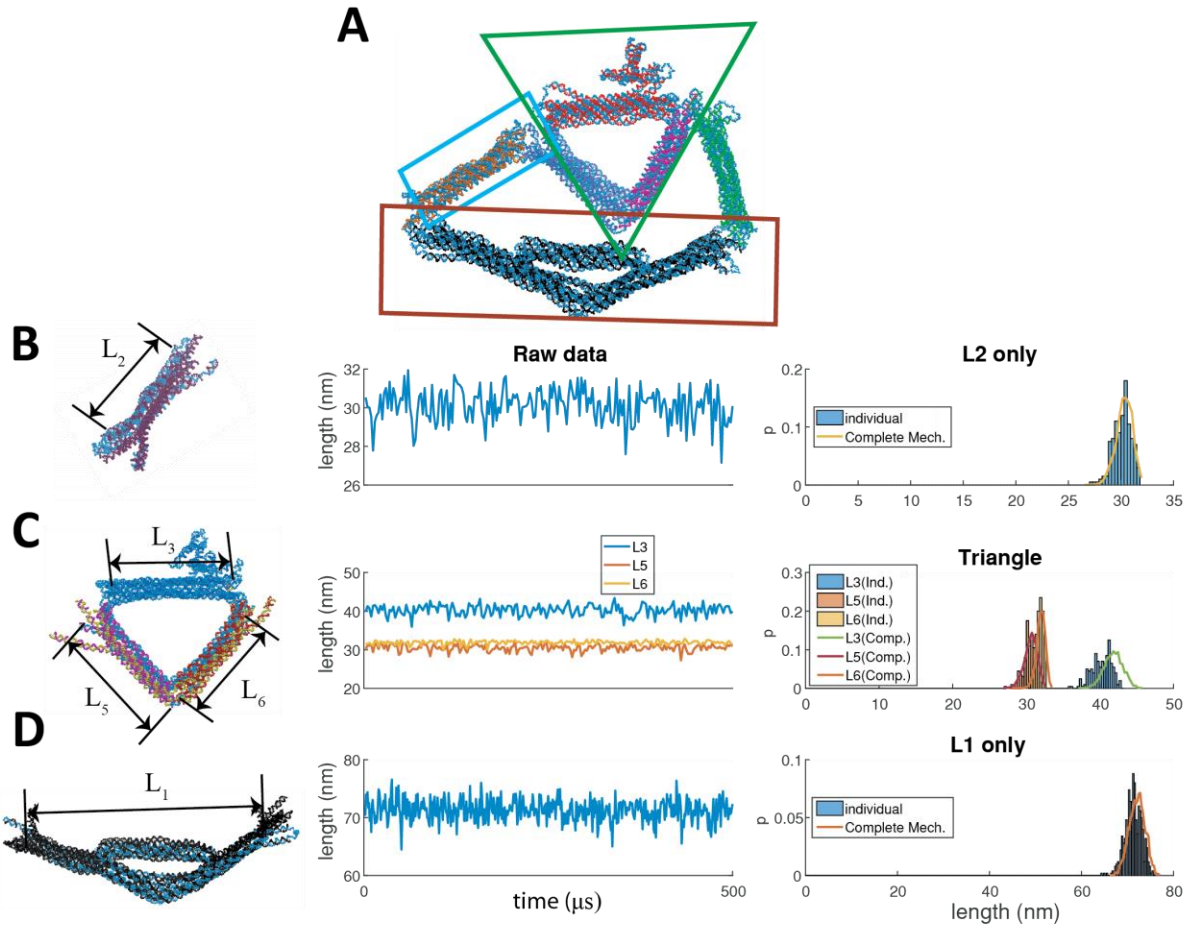

Figure S13: The simulation of individual components as comparison with entire mechanism.(A) schematic of broken pieces. (B)(C)(D) The case of link 2 only, the case of the triangle formed by link 3, link 5, and link 6, and the case of link 1 only, respectively. From left row to right: snapshot of the components, time dependence of the link end-to-end distances, probability distribution (histogram) and comparison with the data from the entire linkage (curve).

f. Fitted models and length distribution of each link

Nomenclature for this subsection:

d_i : end-to-end 3D distances from oxDNA

α_i : out-of-plane angles from oxDNA

$p(\hat{L}_i^{pl}) = f(\hat{L}_i^{pl}; L_{ci}, L_{pi})$

$p(\tilde{L}_i^{pl}) = g(p(d_i), p(\cos\alpha_i)) = g(f(d_i; L_{ci}, L_{pi}), f(\alpha_i; \sigma_{\alpha i}, \mu_{\alpha i}))$

$p(\hat{L}_i^{sk}) = f(\hat{L}_i^{sk}; k_i, \sigma_i, \mu_i)$

$p(\tilde{L}_i^{sk}) = g(p(d_i), p(\cos\alpha_i)) = g(f(d_i; k_i, \sigma_i, \mu_i), f(\alpha_i; \sigma_{\alpha i}, \mu_{\alpha i}))$

We noticed two major geometric errors at the component level in the trajectory files. However, since the experimental TEM images are in 2D, we needed to consider these two errors together by sampling in-plane lengths of each link for subsequent kinematic analysis. To further analytically express the simulation results, we fitted the end-to-end distances with two probability density functions: semi-flexible polymer and a skewed Gaussian distribution. The first one was based on the model created by Thirumalai and Ha[8] shown in equation (S1), where L_c is the contour length, L_p is the persistence length, d is the end-to-end distance, and A is the normalization constant to satisfy the integration of probability as one. The semi-flexible polymer model has two physical parameters L_c and L_p while the skewed Gaussian distribution has three parameters: k, σ and μ .

$$P(L^{pl}) = f(L^{pl}; L_{c,} L_p) = \frac{A \times 4\pi d^2}{L_c{}^2 (1-(d/L_c)^2)^{9/2}} \times \exp\left(\frac{-3L_c}{4L_p(1-(d/L_c)^2)}\right) \quad \text{(S1)}$$

In addition, there are two options for curve fitting and projecting 3D lengths. For the first option, we first project the link onto the reference plane and then fit the distributions of 2D lengths using

both models. This approach is denoted by the hat superscript. The second option (denoted with a tilde superscript) treated those two errors as completely independent sources. We fitted the out-of-plane motion with the normal distribution and fitted the 3D end-to-end distribution with corresponding probability functions. Using the parameters from the fitting, we obtained a sample of 2D lengths by the product of the randomly generated 3D length and the cosine of the randomly generated angle.

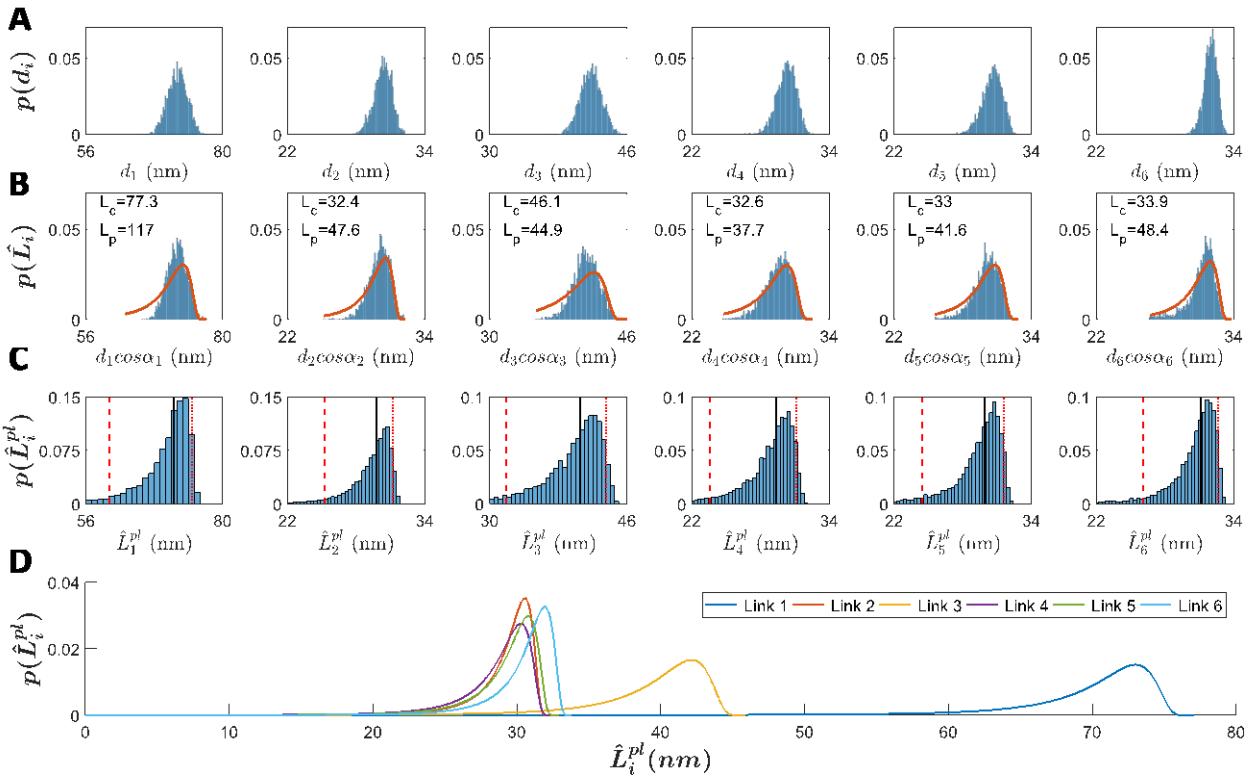

Figure S14: Projecting 3D end-to-end distances to the reference plane first and fitting the 2D length distribution by the semi-flexible polymer model. (A) Histograms of 3D end-to-end distances. (B) Histograms of the projected lengths within the plane for each link. (C) and (D) Reproducing the lengths distribution with the 2 fitting parameters (L_c and L_p from semi-flexible polymer distribution for 2D lengths) for all six links.

Table S2: Statistics of the length populations in Figure S14, unit: nm

$\hat{L}_i^{pl}$	L1	L2	L3	L4	L5	L6
5%	60.2	25.0	31.9	23.6	24.7	26.4
50%	71.3	29.8	40.5	29.3	29.9	31.1
95%	74.6	31.2	43.5	31.1	31.6	32.6

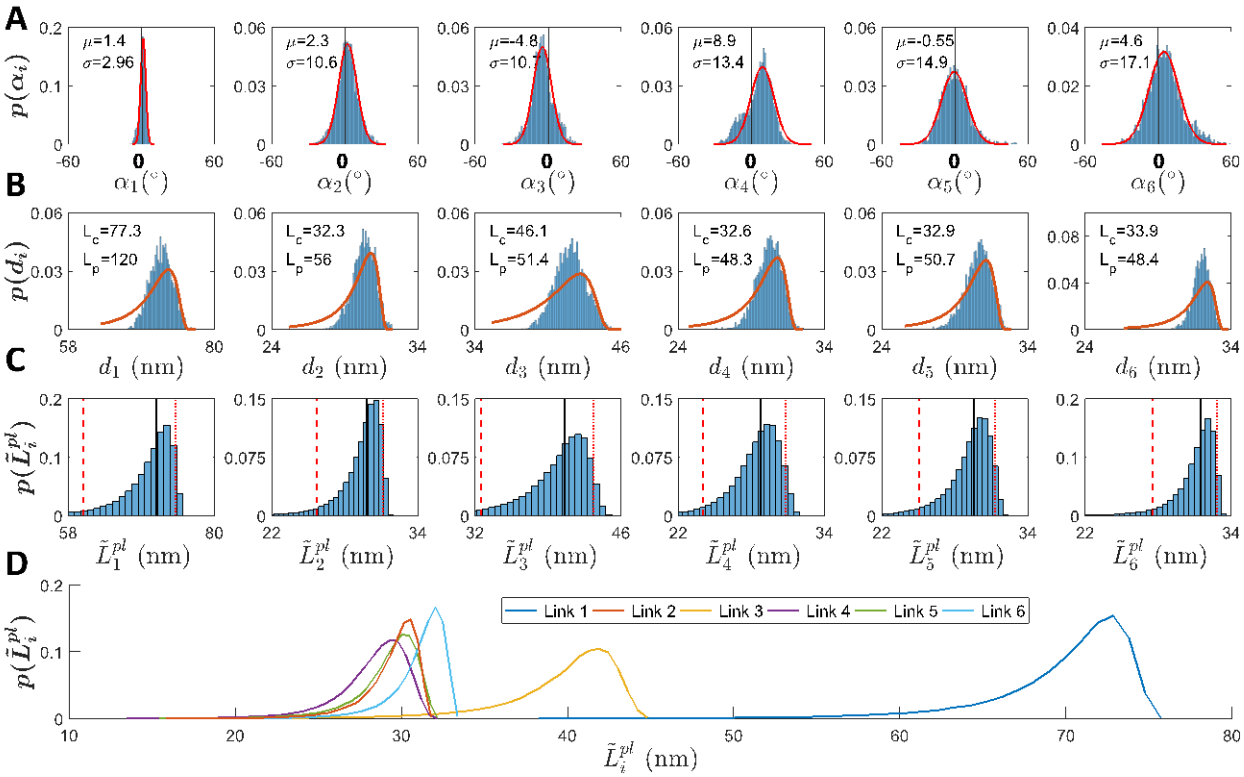

Figure S15: Independently fitting the out-of-plane motion and end-to-end distances with the semi-flexible polymer model. (A) Histograms of the out-of-plane motion for each link and fitted curves by the normal distribution. (B) Histograms of the 3D end-to-end distances and fitted curves by the semi-flexible polymer model. (C)(D) Reproducing the lengths distribution with the 4 fitting parameters (σ and μ from the normal distribution for tilting; L_c and L_p from semi-flexible polymer distribution for 3D lengths) for all six links.

Table S3: Statistics of the length populations in Figure S15, unit: nm

$\tilde{L}_i^{pl}$	L1	L2	L3	L4	L5	L6
5%	60.3	25.7	32.6	24.0	25.0	27.4
50%	71.2	29.8	40.5	28.7	29.6	31.5
95%	74.2	31.2	43.4	30.8	31.3	32.8

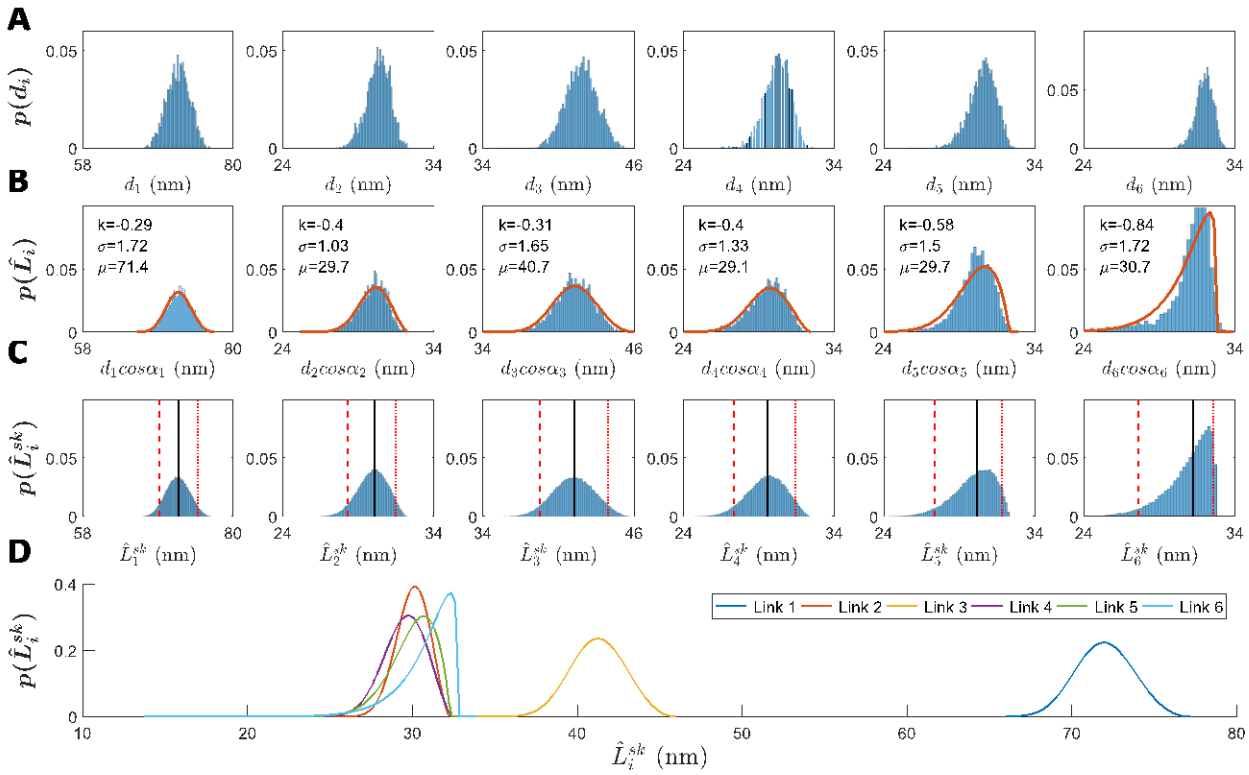

Figure S16: Projecting 3D end-to-end distances to the reference plane first and then fitting the 2D length distribution using the skewed Gaussian model. (A) Histograms of 3D end-to-end distances. (B)Histograms of the projected lengths on the plane for each link. (B)(C) Reproducing the lengths distribution with the 3 fitting parameters (k, σ and μ from the skew-Gaussian distribution for 2D lengths) for all six links.

Table S4: Statistics of the length populations in Figure S16, unit: nm

$\hat{L}_i^{sk}$	L1	L2	L3	L4	L5	L6
5%	69.2	28.3	38.5	27.3	27.4	27.6
50%	72	30	41.2	29.6	30.2	31.2
95%	74.8	31.5	43.9	31.4	31.9	32.6

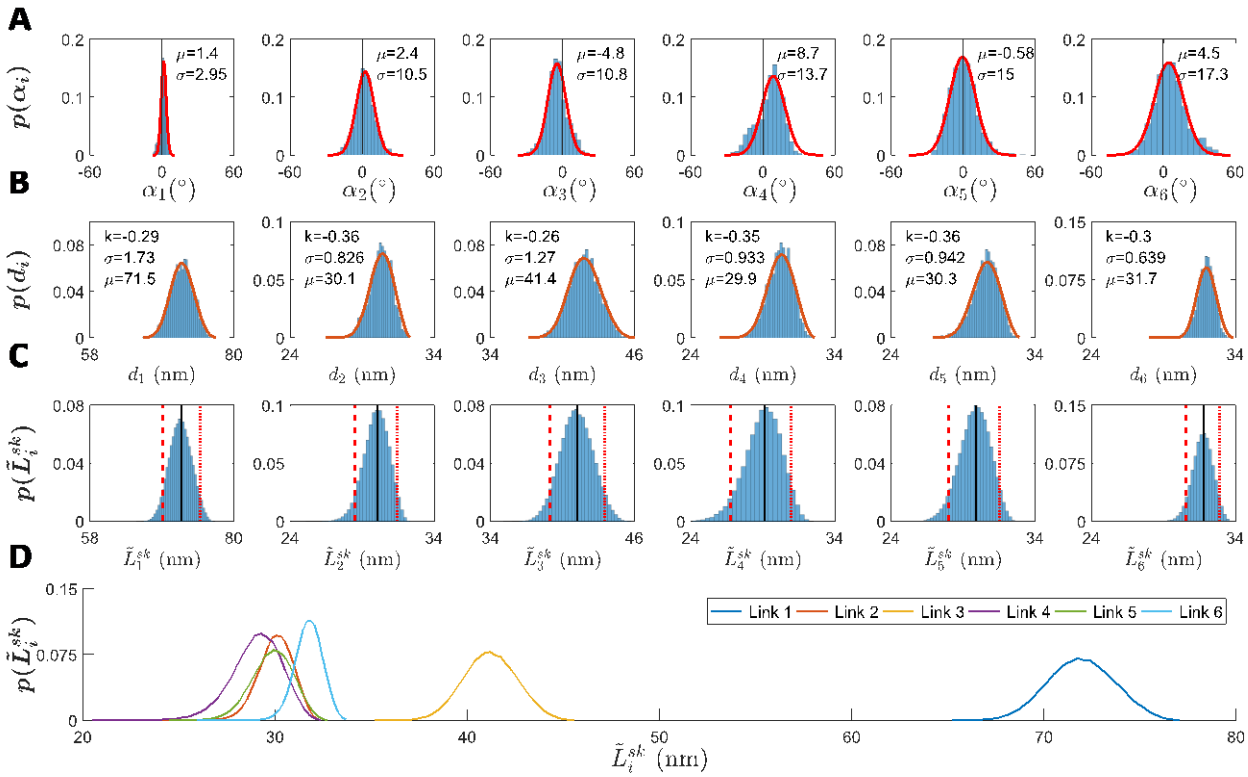

Figure S17: Independently fitting the out-of-plane motion and end-to-end distances using the skewed Gaussian distribution. (A) Histograms of the out-of-plane motion for each link and normal distribution fitted curves. (B) Histograms of the 3D end-to-end distances and skewed Gaussian distribution fitted curves. (C)(D) Reproduced length distributions with the 5 fitting parameters (σ and μ from the normal distribution for tilting; k , σ and μ from the skew-Gaussian distribution for 3D lengths) for all six links.

Table S5: Statistics of the length population in Figure S17, unit: nm

$\tilde{L}_i^{sk}$	L1	L2	L3	L4	L5	L6
5%	69.1	28.5	38.9	26.7	28	30.5
50%	71.9	30.1	41.2	29.1	29.9	31.7
95%	74.8	31.4	43.5	31	31.5	32.9

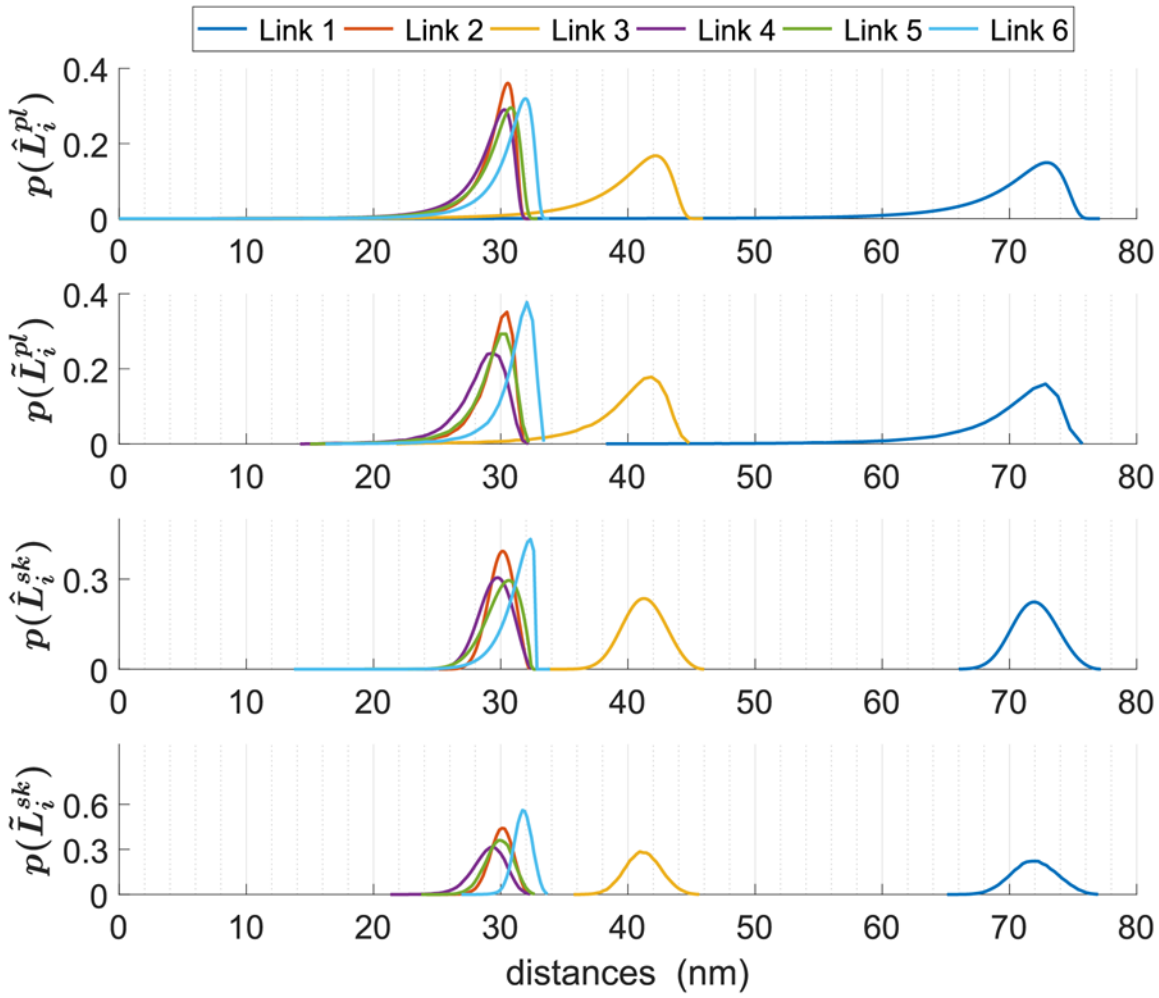

Figure S18: Comparison of reproduced length populations of each fitting model and projection approach from Figure S14-S17

4. Kinematic variance analysis

a. Analytical solution to the kinematic analysis of the closed-loop 4-bar mechanism

Planar four-bar linkages, such as the SLL (Figure S19), are widely used for generating desired motions in macroscopic machines. The kinematic analysis of the constrained motion of four-bar mechanisms is solving the following vector loop equations,

$$l_2 e^{i\theta_2} + l_3 e^{i\theta_3} = l_1 e^{i\theta_1} + l_4 e^{i\theta_4} \quad (S2)$$

Numerous authors have provided analytical solutions to this classical problem. One of them[9] is described here. Note that the four-bar linkage is a mechanism with one degree-of-freedom, which requires an input angle θ_3 to specify the location on the trajectory along with all six well-known links lengths. Our kinematic variance analysis methods are based on this analytical solution in which the lengths would come from the six link lengths distributions from the oxDNA simulation results.

$$A_0 = 2l_1 l_4 \cos\theta_1 - 2l_3 l_4 \cos\theta_3 = f(l_1, l_3, l_4, \theta_3) \quad (S3)$$

$$B_0 = 2l_1 l_4 \sin\theta_1 - 2l_3 l_4 \sin\theta_3 = f(l_3, l_4, \theta_3) \quad (S4)$$

$$C_0 = l_1^2 + l_3^2 + l_4^2 - l_2^2 - 2l_1 l_3 \cos(\theta_1 - \theta_3) = f(l_1, l_2, l_3, l_4, \theta_3) \quad (S5)$$

$$\theta_4 = 2\tan\left[\frac{-B_0 + \sigma\sqrt{B_0^2 + C_0^2 - A_0^2}}{C_0 - A_0}\right],\ \sigma = \pm 1 \quad (S6)$$

$$B_0^2 + C_0^2 - A_0^2 > 0 \quad (S7)$$

$$\vec{P}_3 = \frac{1}{2} l_1 e^{i\theta_1} + l_4 e^{i\theta_4} - l_3 e^{i\theta_3} + l_5 e^{i(\theta_3 - \alpha)} = f(l_1, l_2, l_3, l_4, l_5, l_6, \theta_3) \quad (S8)$$

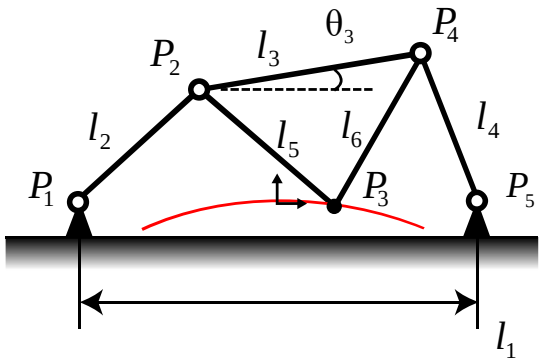

Figure S19: Schematic of the four-bar linkage with four revolute joints at points P_1, P_2, P_4 and P_5.

b. Taylor series expansion with optimization algorithm (TSOA)

The goal of variational kinematic analysis of a given mechanism is to determine the probability distribution of studied kinematic parameters (e.g. trajectory of a point) with given variations of individual parameters (e.g. link lengths). Many authors have studied variational kinematic analysis for macroscopic linkages[10]. The basic method is to first derive Taylor series expansion of studied kinematic parameters in terms of individual parameters and then substituting variations of individual parameters to calculate the probability distribution of studied kinematic parameters. However most of these work only study the first-order model which assumes small variations. Due to significant geometric variations in links and joints made of DNA materials, here we must derive both the first-order and the second-order models for accurately predicting variations of kinematic motions of DNA origami mechanisms.

- First-order model

Figure 4A shows the schematic of this method in which we first used the analytical solution of (8) and the 50th percentile of each link lengths to plot the trajectory as reference. The boundary

of the input-angle θ_3 was determined by the minimum and maximum angles from compiled oxDNA simulations. According to Taylor series expansion, any point $\vec{P}_3$ on the trajectory has a close and approximated point $\vec{P}_3^*$ expressed as:

$$\begin{aligned}\vec{P}_3^* &= \vec{P}_3 + \frac{\partial \vec{P}_3}{\partial l_1}\Delta l_1 + \frac{\partial \vec{P}_3}{\partial l_2}\Delta l_2 + \frac{\partial \vec{P}_3}{\partial l_3}\Delta l_3 + \frac{\partial \vec{P}_3}{\partial l_4}\Delta l_4 + \frac{\partial \vec{P}_3}{\partial l_5}\Delta l_5 + \frac{\partial \vec{P}_3}{\partial l_6}\Delta l_6 \\ &= \vec{P}_3 + (\frac{\partial \vec{P}_3}{\partial l_1}, \frac{\partial \vec{P}_3}{\partial l_2}, ..., \frac{\partial \vec{P}_3}{\partial l_6}) \cdot (\Delta l_1, \Delta l_2, ..., \Delta l_6)^T = \vec{P}_3 + \nabla \vec{P}_3 \cdot \beta\end{aligned} \quad (S9)$$

where ∇ is the gradient operator and $\beta = (\Delta l_1, \Delta l_2, ..., \Delta l_6)^T$ is the length variance vector with the lower bounds (*lb*) and the upper bounds (*ub*) at the 5th and 95th percentiles of each link with reference to the 50th percentiles, respectively. Note that $\nabla \vec{P}_3 \cdot \beta$ is a linear combination of a set of the known first order derivatives multiplied by the optimization variable β. Because the goal of TSOA is to find the boundary of the tip position with varying link lengths, we set the objective function to maximize the projection of the summed vector along the direction of interest $\hat{e}_k$, which was then rotated about $\vec{P}_3$ to in 10^o increments iteratively search the boundary. This first-order optimization problem can be expressed as following:

$$\begin{aligned}&\max_{\beta_i \in [lb, ub]} f = (\nabla \vec{P}_3 \cdot \beta) \cdot \hat{e}_k \\ &s.t.\ (\nabla \vec{P}_3 \cdot \beta) \,||\, \hat{e}_k\end{aligned}$$

- Second-order model

Similarly, one can extend the first-order model to the second-order model by introducing the second order term:

$$\vec{P}_3^* = \vec{P}_3 + \nabla \vec{P}_3 \cdot \beta + \frac{1}{2}\beta^T \cdot \nabla^2 \vec{P}_3 \cdot \beta \quad (S10)$$

where ∇^2 is the Laplace operator. Again, the objective function and the constraint need to be revised as following:

$$\max_{\beta_i \in [lb,ub]} f = (\nabla \vec{P}_3 \cdot \beta + \frac{1}{2}\beta^T \cdot \nabla^2 \vec{P}_3 \cdot \beta) \cdot \hat{e}_k$$

$$s.t.\ (\nabla \vec{P}_3 \cdot \beta + \frac{1}{2}\beta^T \cdot \nabla^2 \vec{P}_3 \cdot \beta) \,||\, \hat{e}_k$$

Figure S20 shows the process of this algorithm in which we used the MATLAB function *fmincon* to solve this non-linear objective function. The result of this method is a potential bounded location of the tip, P_3. We then used the MATLAB function *alphashape* to convert all points on the boundary into a polygon object. For the discretizing densities 9.89° and 10° of θ_3 and $\hat{e}_k$ as in Figure 4(A), the entire process was completed roughly within 20 seconds without using parallel computing.

Algorithm of TSOA

1. obtain analytical solution of $\vec{P}_3(\theta_3)|_{l_{i,50th}}$
2. derive $\nabla \vec{P}_3(\theta_3)|_{l_{i,50th}}$
3. derive $\nabla^2 \vec{P}_3(\theta_3)|_{l_{i,50th}}$
4. for all θ_3 do
5. subs θ_3 to get $\nabla \vec{P}_3, \nabla^2 \vec{P}_3$
6. for all $\hat{e}_k$ do
7. β = *fmincon*(objfun, β_0, *lb*, *ub*, *nonlcon*)
8. $\vec{P}_3^* = \vec{P}_3 + \nabla \vec{P} \beta + \frac{1}{2}\beta^T \cdot \nabla^2 \vec{P}_3 \cdot \beta$
9. collect all $\vec{P}_3^*$
10. Area =*alphashape*(all $\vec{P}_3^*$)

Figure S20: Pseudo code for TSOA

c. Monte Carlo simulation

Monte Carlo (MC) simulations are widely used when a system has multiple input variables and is hard to solve deterministically. With the analytical solution in Eq. S8 and the link length population in Figure S14-S17, we can calculate the $\vec{P}_3$ repeatedly with one set of link length samples taken from the length length distributions. Moreover, to quantify the effect of the joint error as shown in Figure 3(D), we revised the vector loop equation with four random terms representing the 2-nt ssDNA connections as:

$$l_2 e^{i\theta_2} + l_3 e^{i\theta_3} + r_{12} e^{\theta_{12}} + r_{25} e^{\theta_{25}} = l_1 e^{i\theta_1} + l_4 e^{i\theta_4} + r_{14} e^{\theta_{14}} + r_{46} e^{\theta_{46}} \quad (S11)$$

where r_{ij} and θ_{ij} denote the magnitude and direction of the joint between link i and link j. Next, we further lumped the l_1 term with four random terms as one term as shown in Figure S21:

$$l_2 e^{i\theta_2} + l_3 e^{i\theta_3} = \mathrm{L}_1 e^{i\theta_{L1}} + l_4 e^{i\theta_4} \quad (S12)$$

where $\mathrm{L}_1 e^{i\theta_{L1}} = l_1 e^{i\theta_1} + r_{14} e^{\theta_{14}} + r_{46} e^{\theta_{46}} - r_{12} e^{\theta_{12}} - r_{25} e^{\theta_{25}}$

Eq. (S12) is similar enough to Eq. (2). Thus, the derivation of the analytical solution from Eq. (S3-S7) can be applied again to obtain the analytical solution of the tip $\vec{P}_3$ with four joint error terms.

$$\vec{P}_3 = \frac{1}{2} L_1 e^{i\theta_{L1}} + r_{14} e^{\theta_{14}} + l_4 e^{i\theta_4} + r_{46} e^{\theta_{46}} - l_3 e^{i\theta_3} + l_5 e^{i(\theta_3 - \alpha)} \quad (S13)$$

Either using the 50th percentiles of each link as a constant rigid link or setting r_{ij} equal to zero, we can isolate the joint and the link errors, respectively, as shown in Figure 4B.

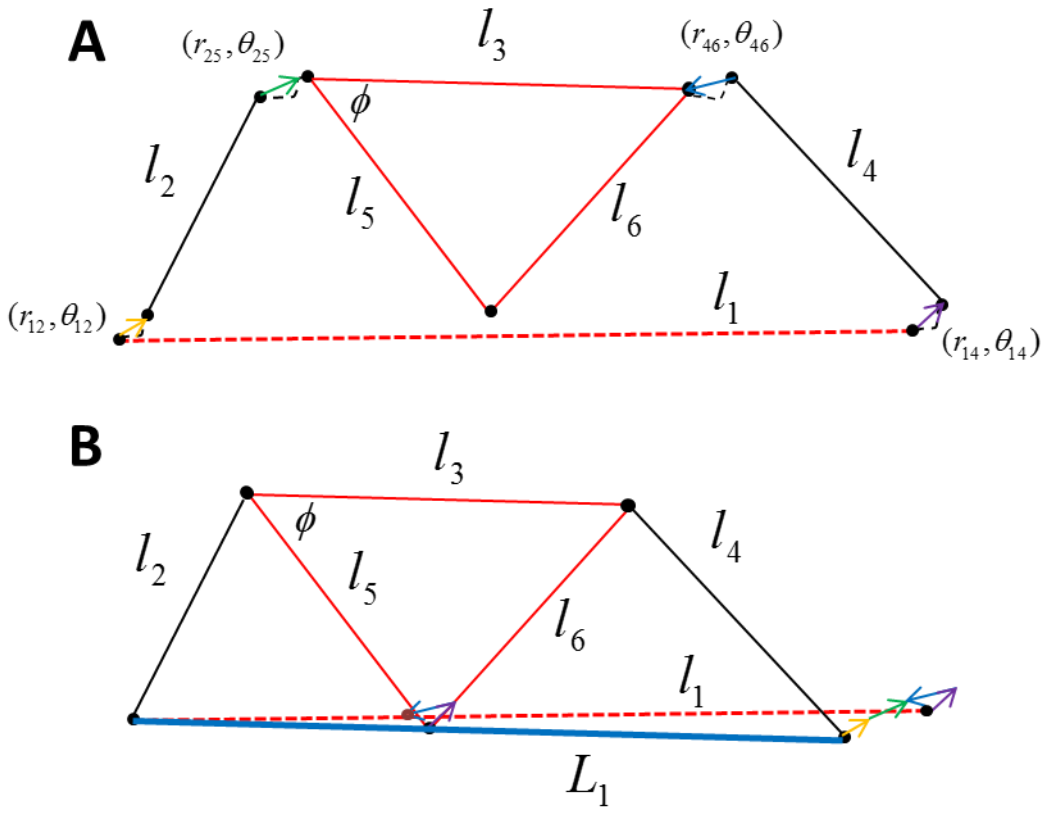

Figure S21: Schematic of the modified vector loop for a four-bar linkage with joint errors. (A) Due to the joint error, one end of a link does not coincide with one end of another link. (B) The vector loop equation is still valid with the extra four random terms by lumping the original l_1 with four random terms turns this linkage into a classic closed four-bar linkage.

d. Validation with experimental data

We have shown four kinds of length populations from two end-to-end distance models and two projection approaches as shown as Figure S18. We have also utilized two kinds of kinematic variance analyses, TOSA and MC methods, to provide an in-depth analysis of varying link lengths. In Figure S22, we provided four different lengths as inputs to our kinematic methods. In general, we expect a broadly distributed population of lengths would predict a larger area. Among these areas, the semi-flexible polymer fits, $\hat{L}_i^{pl}$ and $\tilde{L}_i^{pl}$, created left tails on the distribution curves. These tails were not present in the original trajectory data, especially for link 1 and link 3, which are not defined as the end-to-end distances of a "single" bundle. This resulted in an overestimation of the predicted area. In conclusion, we suggested using the fitting process $\hat{L}_i^{sk}$, which is the length population in Figure 3C and Figure 4.

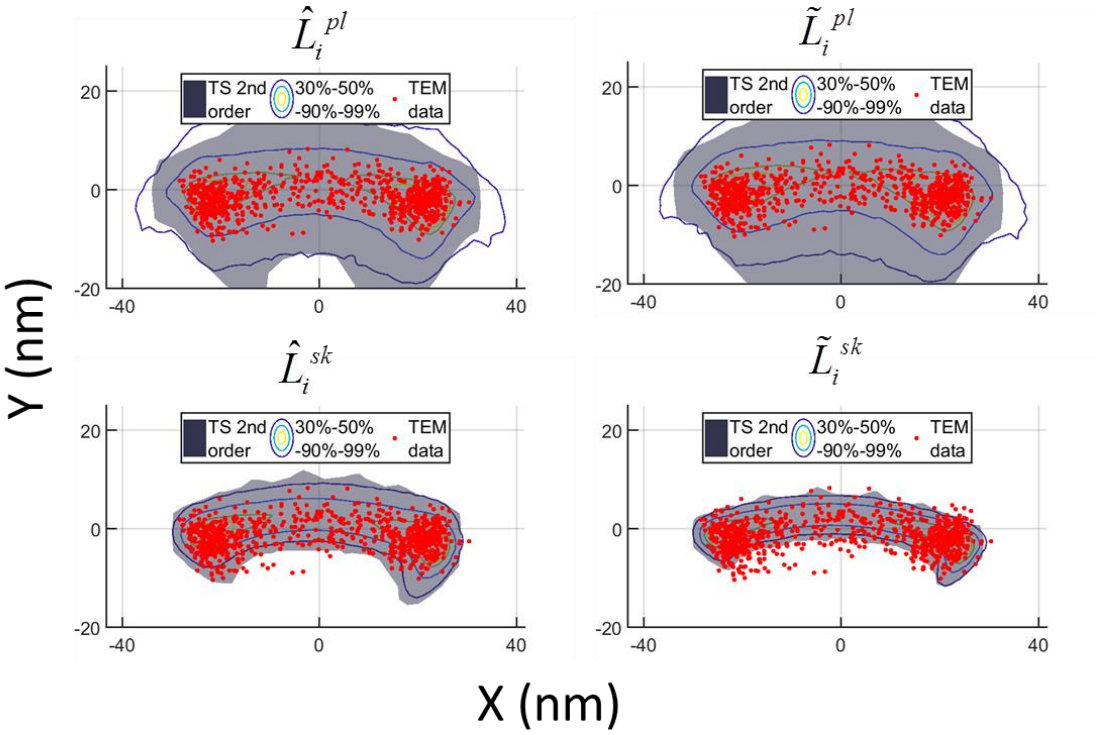

Figure S22: Individually applying two computational methods with four kinds of length populations, verified with experimental data.

Table S6: Repeatability of the stochastic MC method for four contour levels to ensure the sufficiency of the sample size

Levels	$\hat{L}_i^{pl}$	$\tilde{L}_i^{pl}$	$\hat{L}_i^{sk}$	$\tilde{L}_i^{sk}$
30%	43.7±0.2	48.4±0.4	31.6±0.3	17.1±0.2
50%	64.6±0.5	70.8±0.6	46.5±0.4	32.5±0.1
90%	92.2±0.1	98.5±0.0	77.6±0.3	60.7±0.1
99%	1	1	92.6±0.3	80.2±0.4

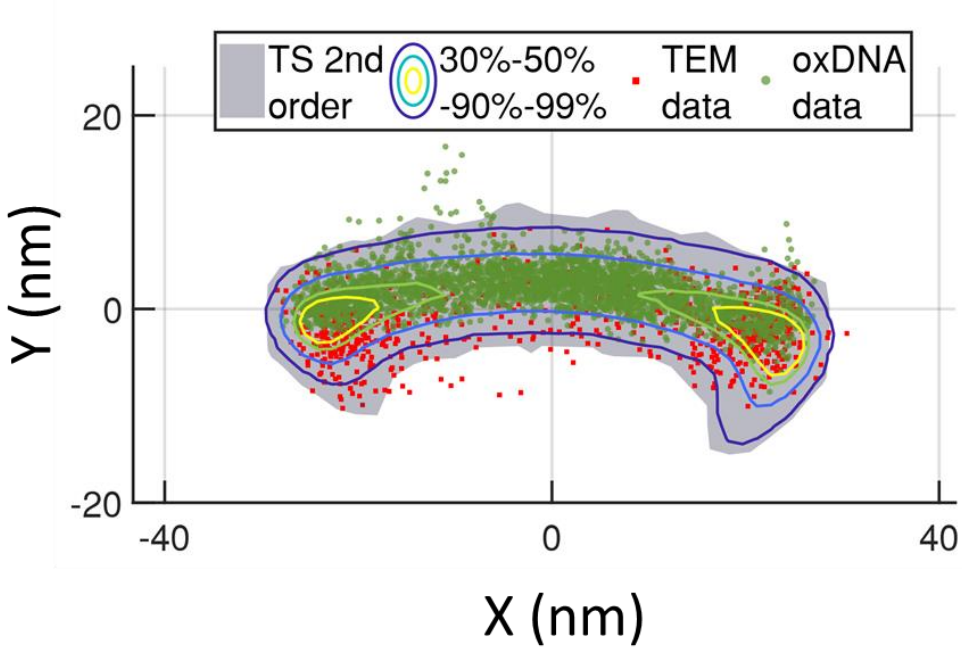

Figure S23: Comparing the experimental, oxDNA simulation, and two computational tools. The two computational results used the links populations $\hat{L}_i^{sk}$

e. The tip prediction using link lengths from individual simulations

So far, we have shown that this hybrid computational tool quantifies the uncertainty by extracting length distributions from all four trajectories of simulations. One may be interested in using the same procedure for individual simulation results since it may reduce the required computational time. Table S7 shows the mean value and standard deviation of length population using the proposed fitting process $\hat{L}_i^{sk}$, a skewed Gaussian distribution. Here, we list the mean values and the standard deviations of the predicted results in Figure S24. The mean values are quite close and the standard deviations reflect the widths of the predicted areas. Note this hybrid tool still needs to perform at least two simulations starting at both sides to determine the range of θ_3.

Table S7: Statistics of each link length from four repeated simulations

Trajectory		L_1	L_2	L_3	L_4	L_5	L_6
center-short	$<\hat{L}_i^{sk}>$	72.4	30.1	41.4	30.0	29.0	31.1
	$\sigma_{\hat{L}_i^{sk}}$	1.76	0.92	1.34	1.13	2.15	1.27
left-short	$<\hat{L}_i^{sk}>$	72.3	30.2	41.5	30.2	29.5	31.5
	$\sigma_{\hat{L}_i^{sk}}$	1.65	0.87	1.29	1.0	1.23	0.85
right-short	$<\hat{L}_i^{sk}>$	71.3	29.9	41.4	29.1	30.3	30.9
	$\sigma_{\hat{L}_i^{sk}}$	1.55	0.96	1.59	1.15	1.05	1.47
center-long	$<\hat{L}_i^{sk}>$	71.9	29.9	41.0	29.2	30.3	30.5
	$\sigma_{\hat{L}_i^{sk}}$	1.70	1.03	1.74	1.28	1.03	2.06

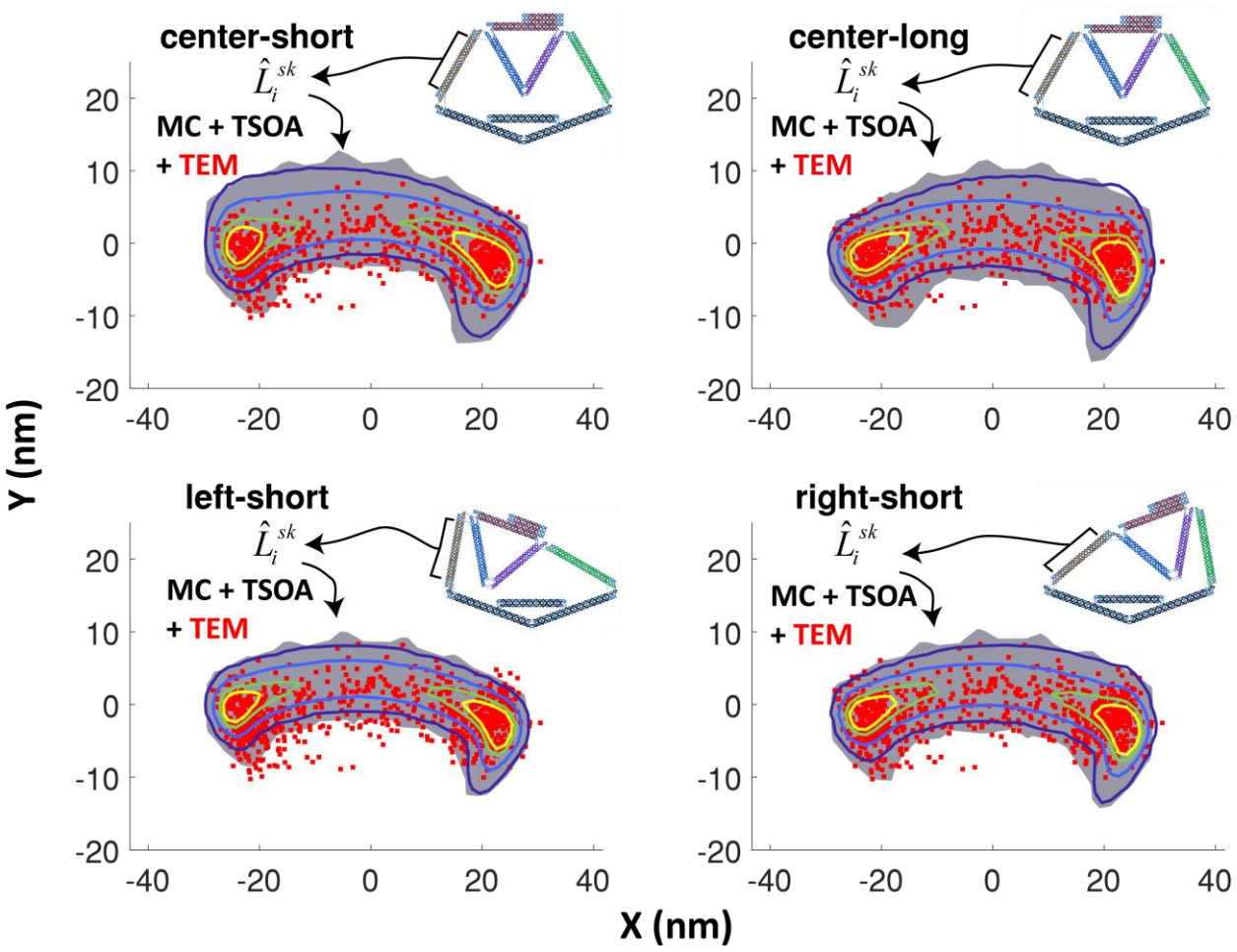

Figure S24: Applying kinematic variance approach to individual simulations.

Table S8: Quantitative comparison of applying kinematic variance approach (MC method) using data from individual simulation trajectories. We set four contour levels, 30%, 50%, 90%, and 99%, for the MC method. The ratio of TEM data falling into the corresponding contour are listed in this table.

Contour level	30%	50%	90%	99%
C-short	28.3%	43.2%	73.3%	88.6%
C-long	31.5%	48.0%	80.2%	93.9%
L-short	22.0%	35.3%	65.2%	82.4%
R-short	26.7%	42.6%	74.0%	89.8%
compiled	30.0%	44.5%	76.2%	91.8%

f. Another case- the crank-slider mechanism

To demonstrate the generality of this proposed hybrid computational tool, we choose the crank-slider mechanism[11,12] as another example. Similarly, we first converted the json file into the oxDNA format by using the python code cadnano_interface.py, rigid body transformed individual links into approximate positions, relaxed the structure, and performed an oxDNA simulation for 1500μs as shown in Figure S25(A). Next, we need to build the kinematic model from the trajectory file. The crank-slider kinematic model has been previously reported[11] as:

$$r(\theta) = a\cos\theta + \sqrt{b^2 - (a\sin\theta - d)^2} - m \tag{S14}$$

where r is the extension, a is the length of the crank, b is the length of the coupler, d is the offset distance, m is the distance from the joint to the close side of the slider, and θ is the crank angle. Originally, these parameters were constant values from the design in the json file. Here, we extract these values from the trajectory, according to Figure S25(B): a and b are link lengths, similarly to the previous approach; d is the difference distances between the two of the joints(P_A and P_C) to the spindle(Point-Line distances); m is the point-plane distance where we selected several bases to fit the plane; θ is the angle between the spindle and the crank link where we only use 60% of the bases on these bundles to avoid the fraying area as Sharma *et al.*[12].. Figure S25(B) and (C) shows the selected bases and the extracted lengths distributions. The Monte Carlo method samples the input-output relationship times as Eq. S14 by using the lengths distributions as Figure S25(C). Figure S25(D) shows the predicted area along with the TEM data from our previous research11 and using two sources of angular distributions, θ from our own simulation and θ_s from longer oxDNA simulations performed on the same mechanism by Sharma *et al.*[12].

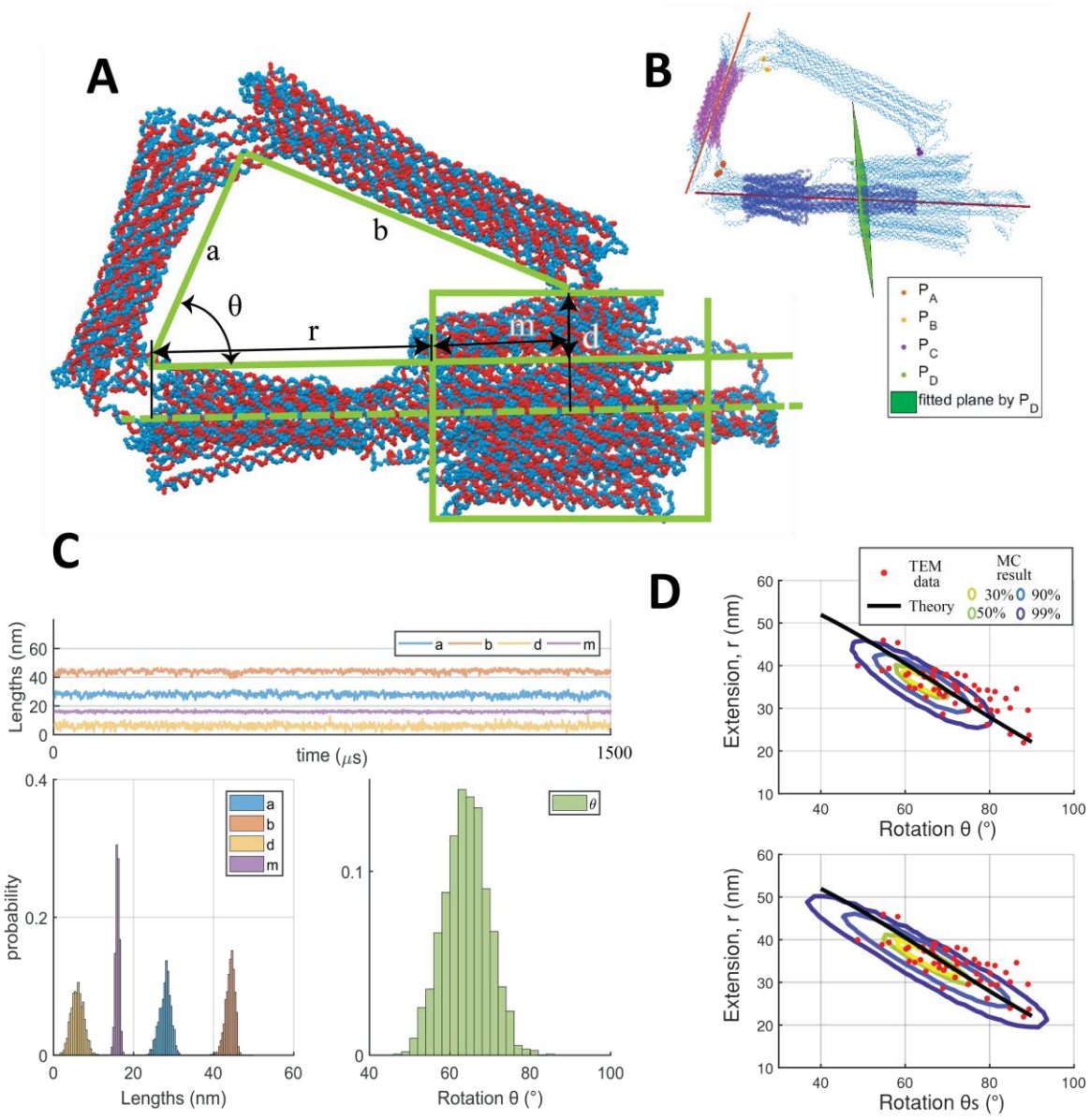

Figure S25: Uncertainty quantification of the crank-slider mechanism[11]. (A) Representative snapshot of the oxDNA simulation. (B) A schematic of extracting the kinematic variable from the simulation. (C) Time-dependence of the kinematic variables. The distributions of these four lengths and the crank-slider angle are the inputs of the kinematic variance analysis. (D) The result of uncertainty quantification using the Monte Carlo method compared with the experiment data[11]. (Top) The rotation angle θ distribution was from this 1500μs simulation. (Bottom) The rotation angle θ_s was generated as Gaussian distribution with $\langle\theta_s\rangle = 65.4°, \sigma_s = 9.3°$ as the previous research by Sharma *et al*[12].

5. DOM conformational probability distribution

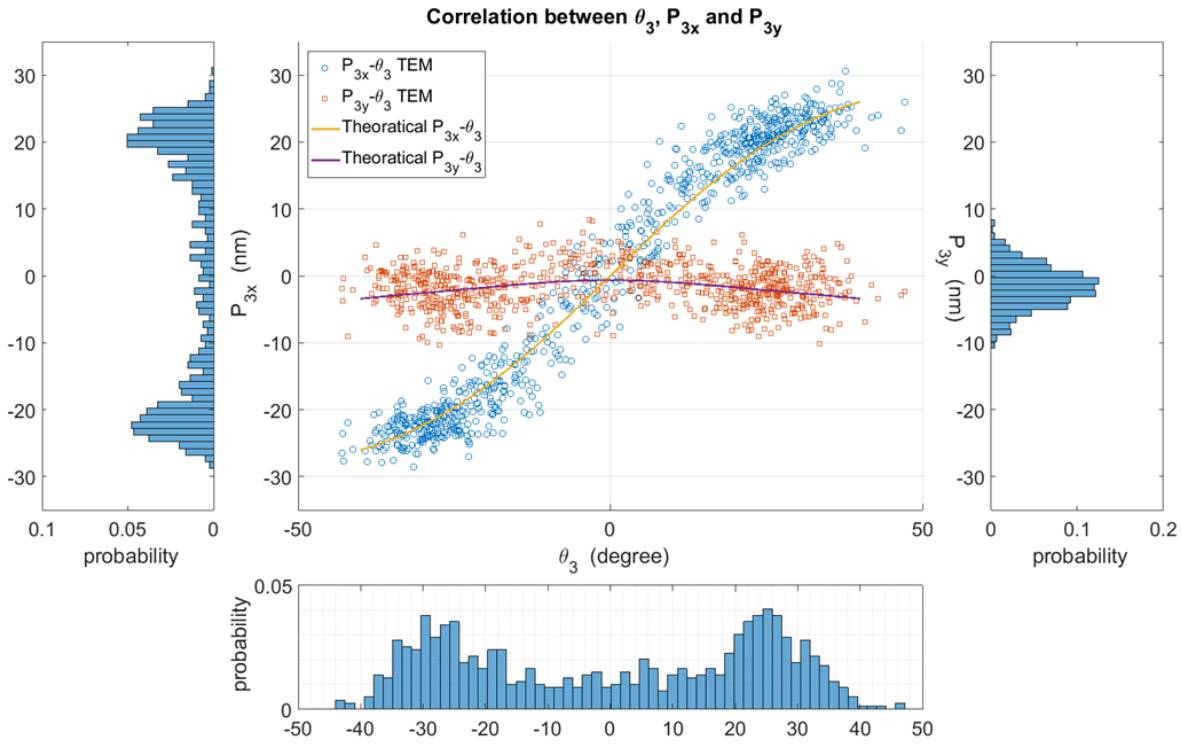

Figure S26: Correlation of the experimental data between θ_3, P_{3x}, and P_{3y} for the SLL with 10mM MgCl2. P_{3x} (left) exhibits stronger bimodal behavior than θ_3 (bottom). Sample size N=791.

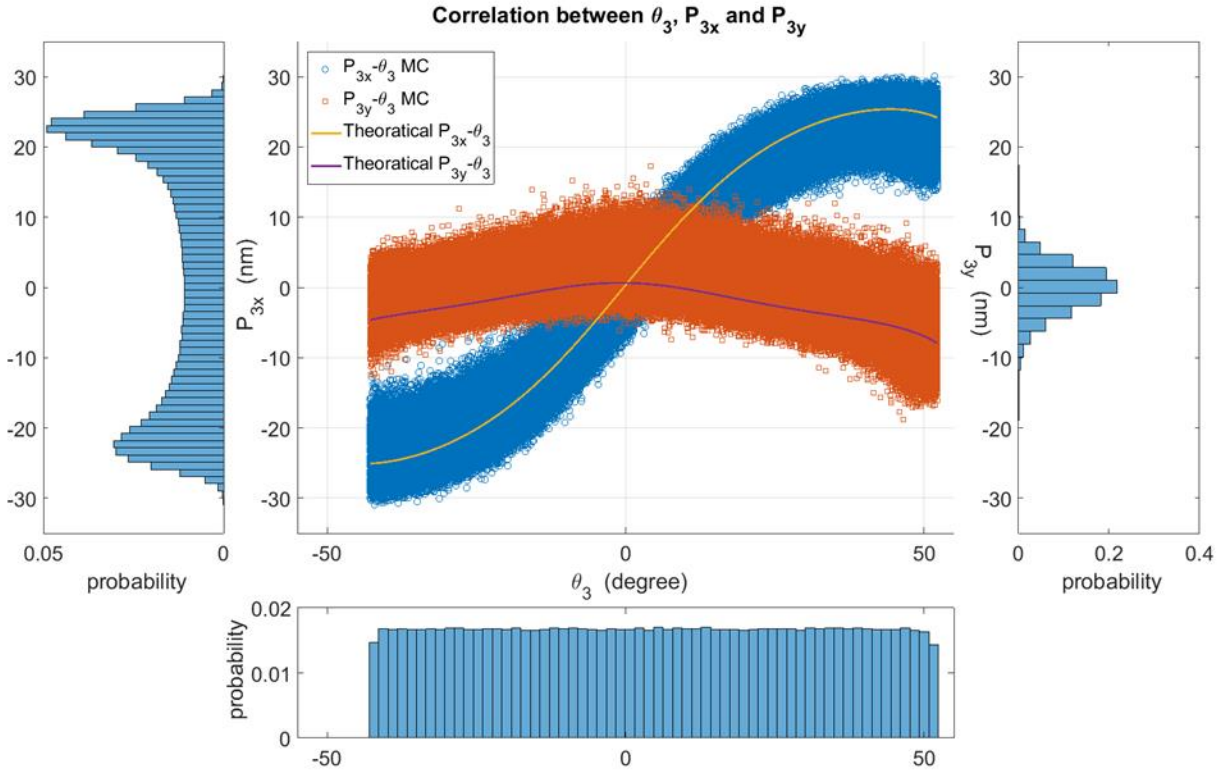

Figure S27: Correlation of the MC sampling. Note the analytical solution of the tip is a function of the six links lengths and the input angle θ_3. The length population came from the simulation results, $\hat{L}_i^{sk}$. The lower and upper bounds of the input angle θ_3 were based on the compiled oxDNA results. Assuming a uniform input angle distribution, The MC sampling of the tip position P_{3x} still shows bimodal behavior (left) with respect to the kinematic solution. This suggests part of the bimodal behavior is due simply to the kinematics of the mechanism. Sample size N=10^6

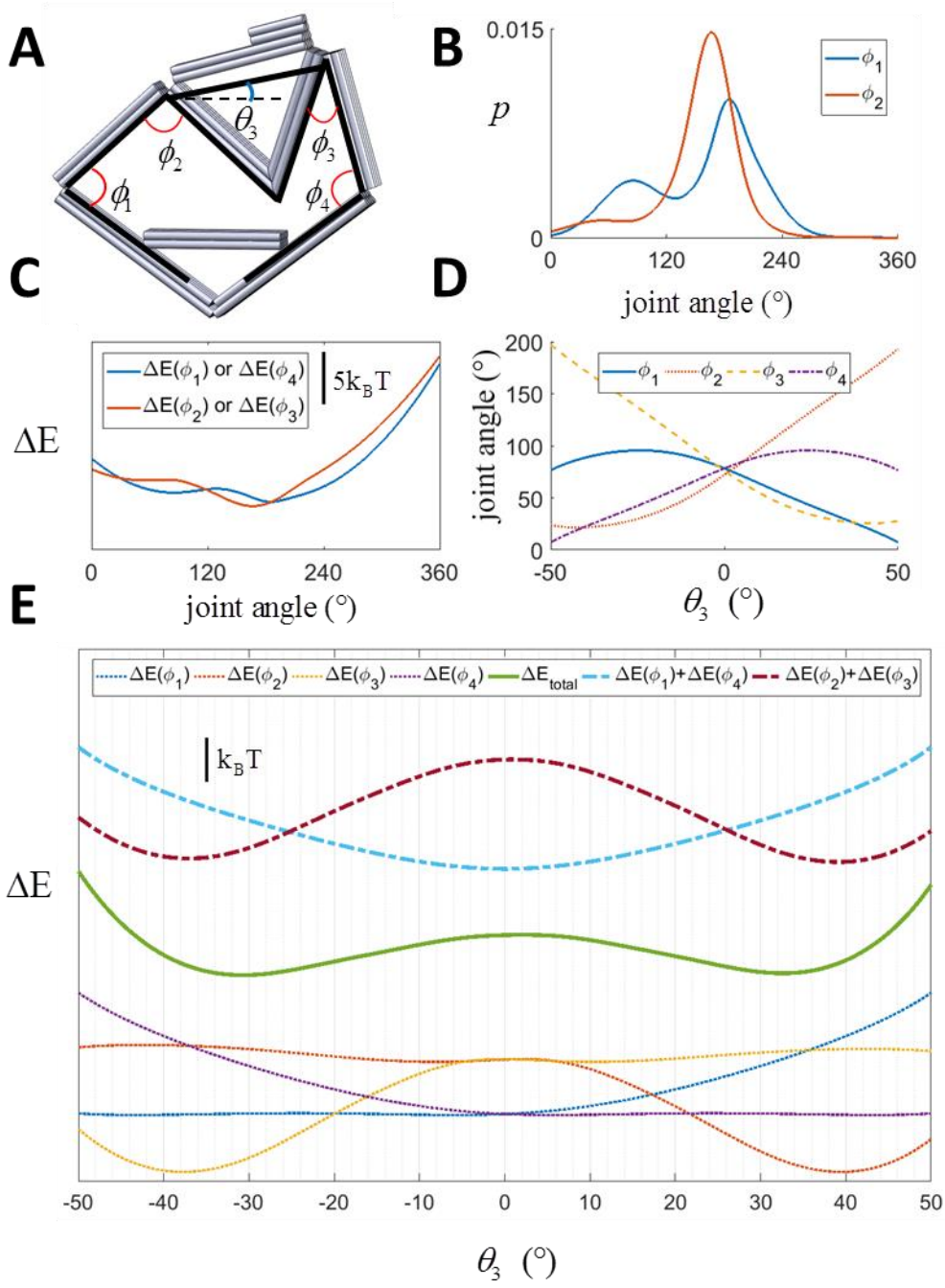

Figure S28: Evaluating the SLL conformational distribution with respect to θ_3 from joint properties determined in the open-chain SLL experiment. (A) Schematic of the angles notations. θ_3 is the absolute angle to the horizontal line in the kinematic analysis. ϕ_i denotes the relative angles between two arms. (B) Probability distributions of the two joints angles excluding the staples on the link 4. (C) The free energy landscape of the two joints calculated with the Boltzmann

distribution. (D) Kinematic analysis from the input angle θ_3 to the four joints' angles ϕ_i. (E) The free energy landscape of each individual joint and summations of multiple joints at different configurations.

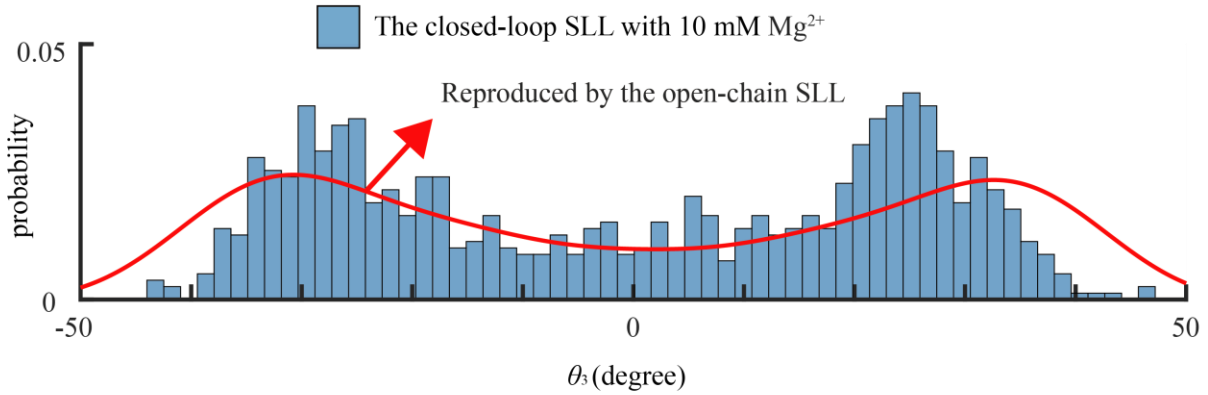

Figure S29: Comparison of θ_3 distributions between the closed-loop SLL experiments (Figure S26) and the reproduced curve (Figure 5F) from the open-chain SLL experiments for comparison.

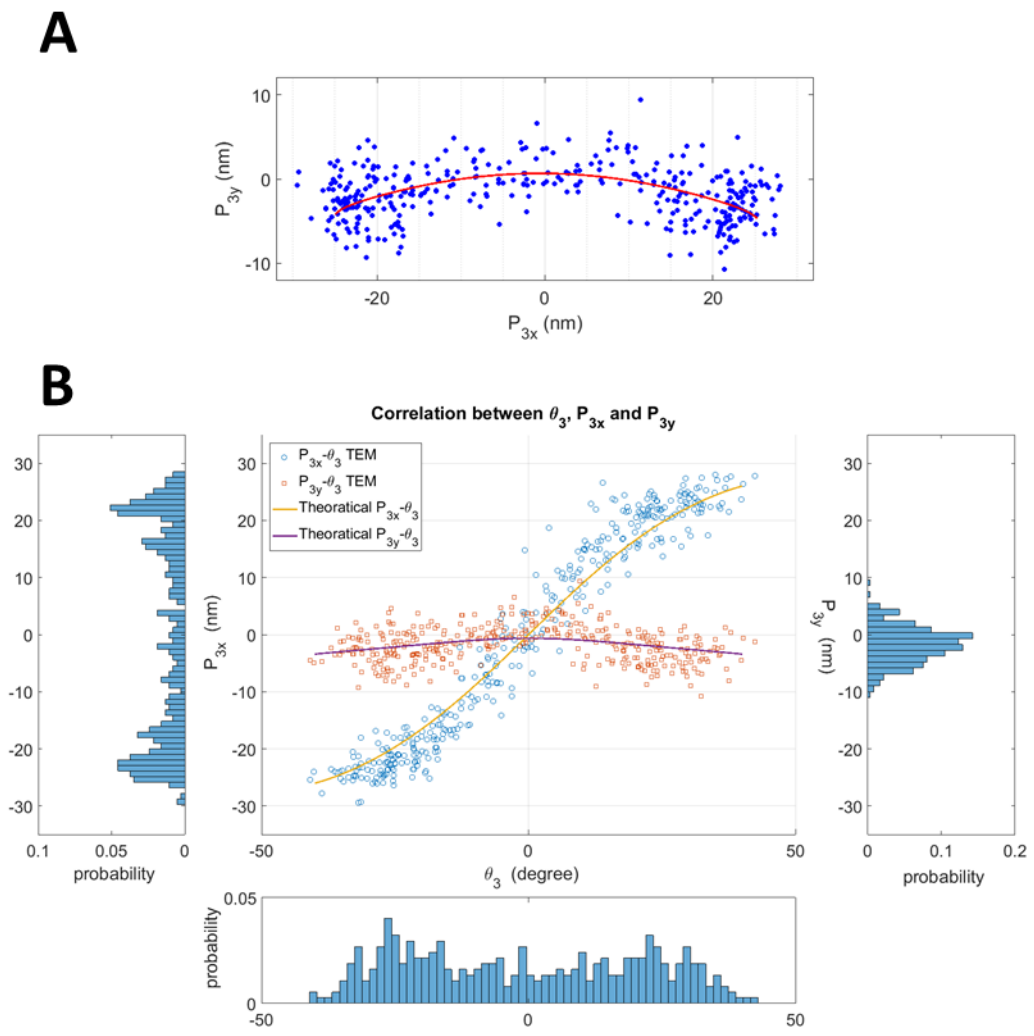

Figure S30: Experimental data for the SLL in 5mM $MgCl_2$. (A) Planar distribution of the tip P_3. (B) Correlation of experimental data for the SLL. Sample size N=373.

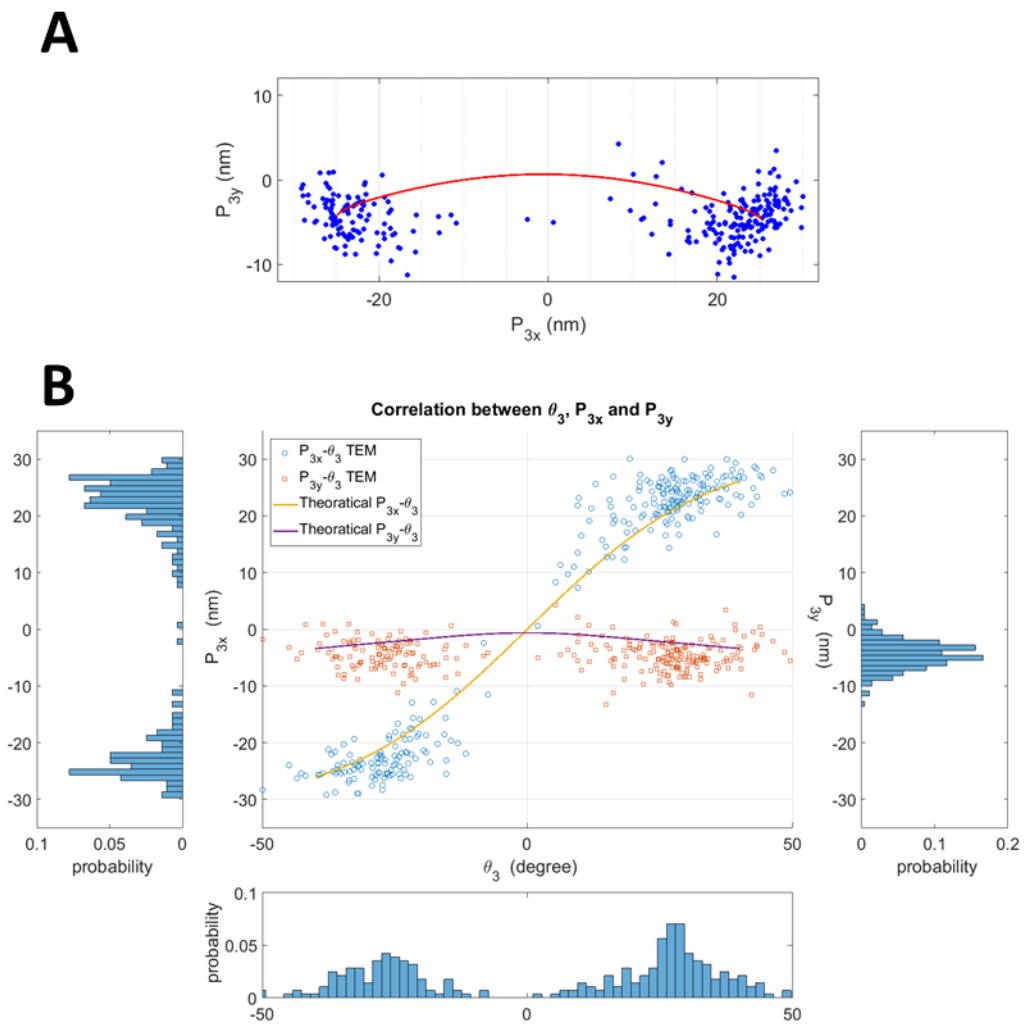

Figure S31: Experimental data for the SLL in 20mM $MgCl_2$. (A) Planar distribution of the tip P_3. (B) Correlation of experimental data of the free SLL. Sample size N=283.

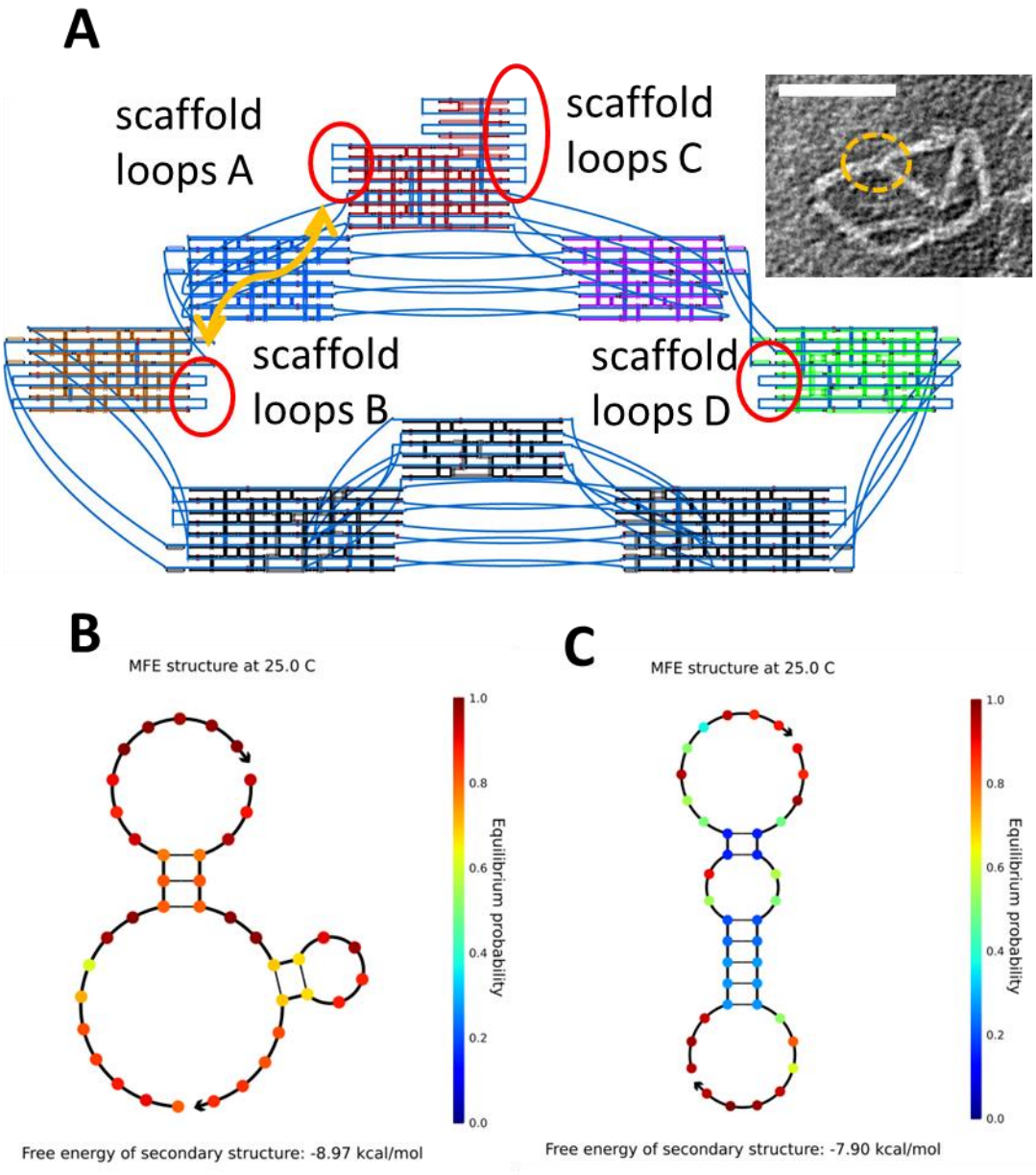

Figure S32 : Single-stranded scaffold loops to lock the joints. (A) Schematic of four groups of ssDNA scaffold loops to prevent intramolecular base-stacking interaction. These sequences were known and had enhanced interaction at high-salt conditions. (B) and (C) Snapshots of NUPACK web-based software[13] predicting secondary structures formed by scaffold loops.

Table S9: Sequences of the 20-nt scaffold loops shown in Figure S32 (A).

Scaf loops	Sequences
A1	CAAGTCGGGAGGTTCGCTAA
A2	GAATATCAAGGCCAATCGTC
B1	AAGTATAATCCAAACAATCA
B2	TTTGCCAACTGACCAGATAT
C1	ATTGCGTTTCCTCGGTTTCC
C2	TAAAAAGGGCTTCGGTAAGA
C3	ACTGCGTAATAAGGAGTCTT
C4	TTTCTTTTATATGTTGCCAC
D1	GTATCTGCATTAGTTGAATG
D2	TCTTTCTACCTGTAATAATG

Table S10: The free energy of secondary structures for all paired scaffold loops from NUPACK. Unit: kcal/mol.

Scaffold loops Pairing	Free energy of secondary structure	Scaffold loops Pairing	Free energy of secondary structure
A1-B1	-6.28	C1-D1	-5.52
A2-B1	-5.02	C1-D2	-6.13
A1-B2	-7.9	C2-D1	-7.02
A2-B2	-8.97	C2-D2	-7.42
		C3-D1	-6.38
		C3-D2	-6.82
		C4-D1	-5.78
		C4-D2	-4.15

6. Gel and Zoom-out TEM images

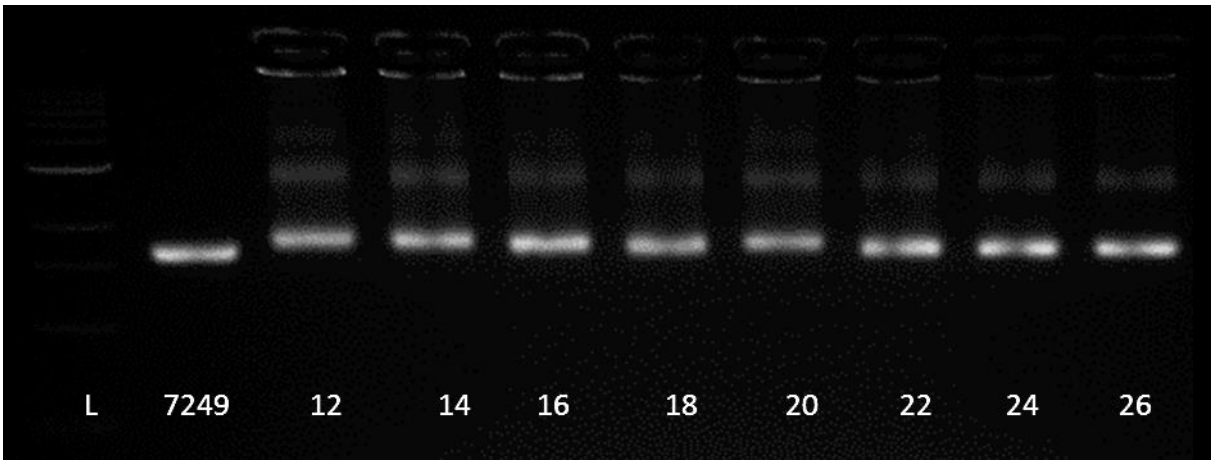

Figure S33: Agarose gel electrophoresis of the SLL after a 2.5 day folding reaction. The lanes from left to right are 1-kb ladder, a scaffold reference (p7249), and a salt gradient from 12 to 26 mM $MgCl_2$.

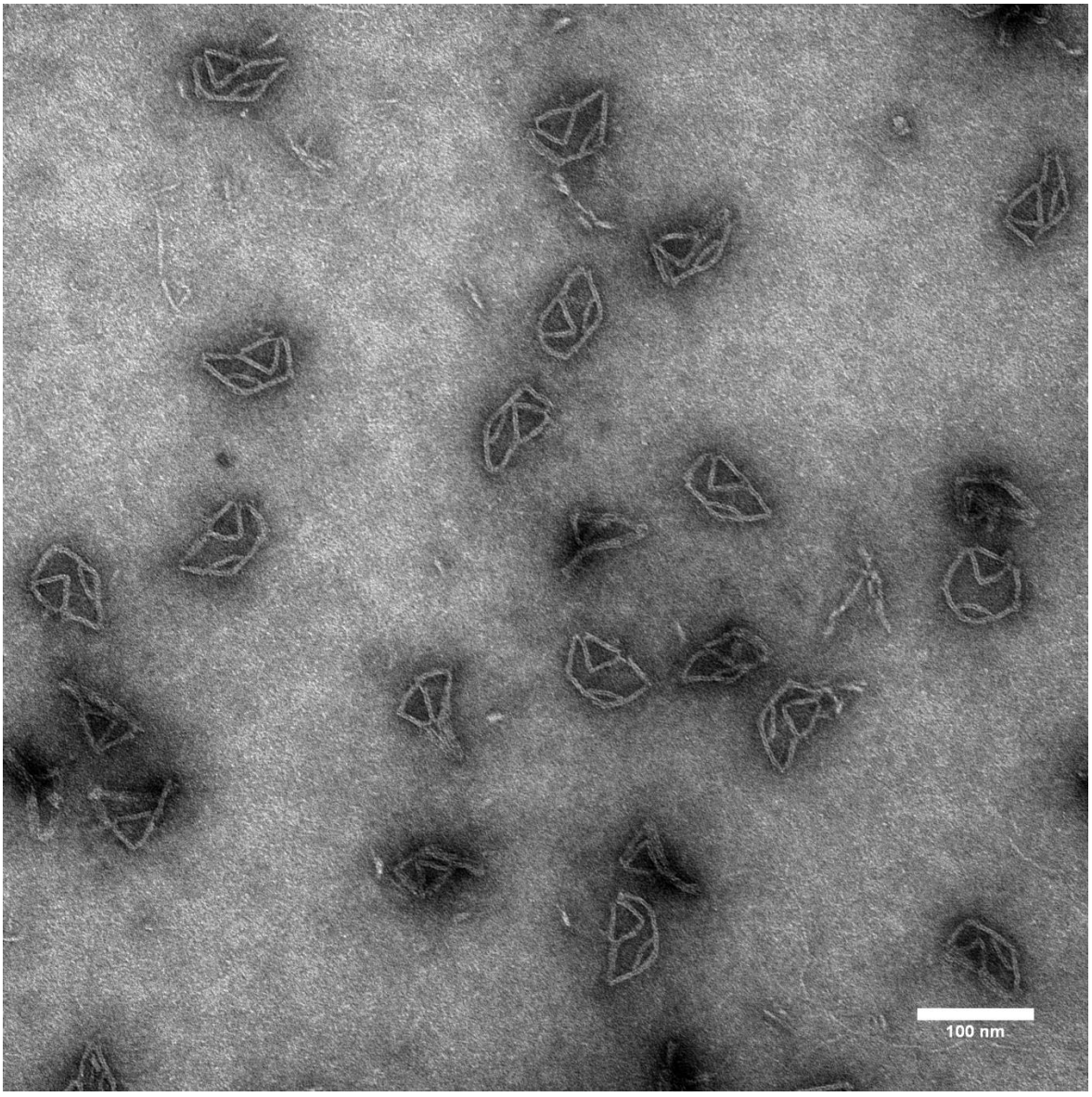

Figure S34: TEM image of the SLL after agarose gel electrophoresis purification in 10mM $MgCl_2$ buffer.

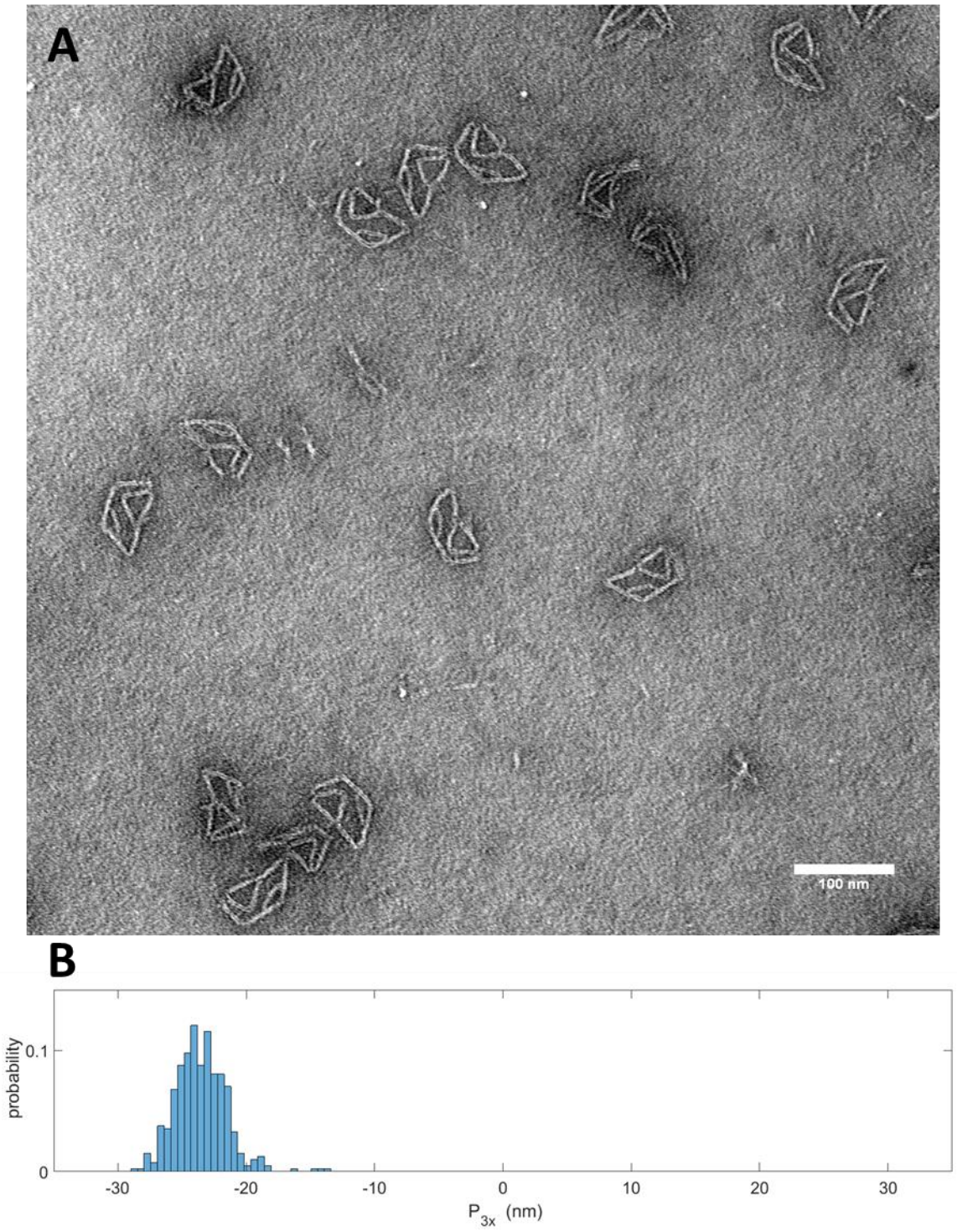

Figure S35: (A) TEM image of the SLL actuated to the left, opposite to the marker side after agarose gel electrophoresis purification in 10mM $MgCl_2$ buffer. (B) Horizontal distribution of the tip.

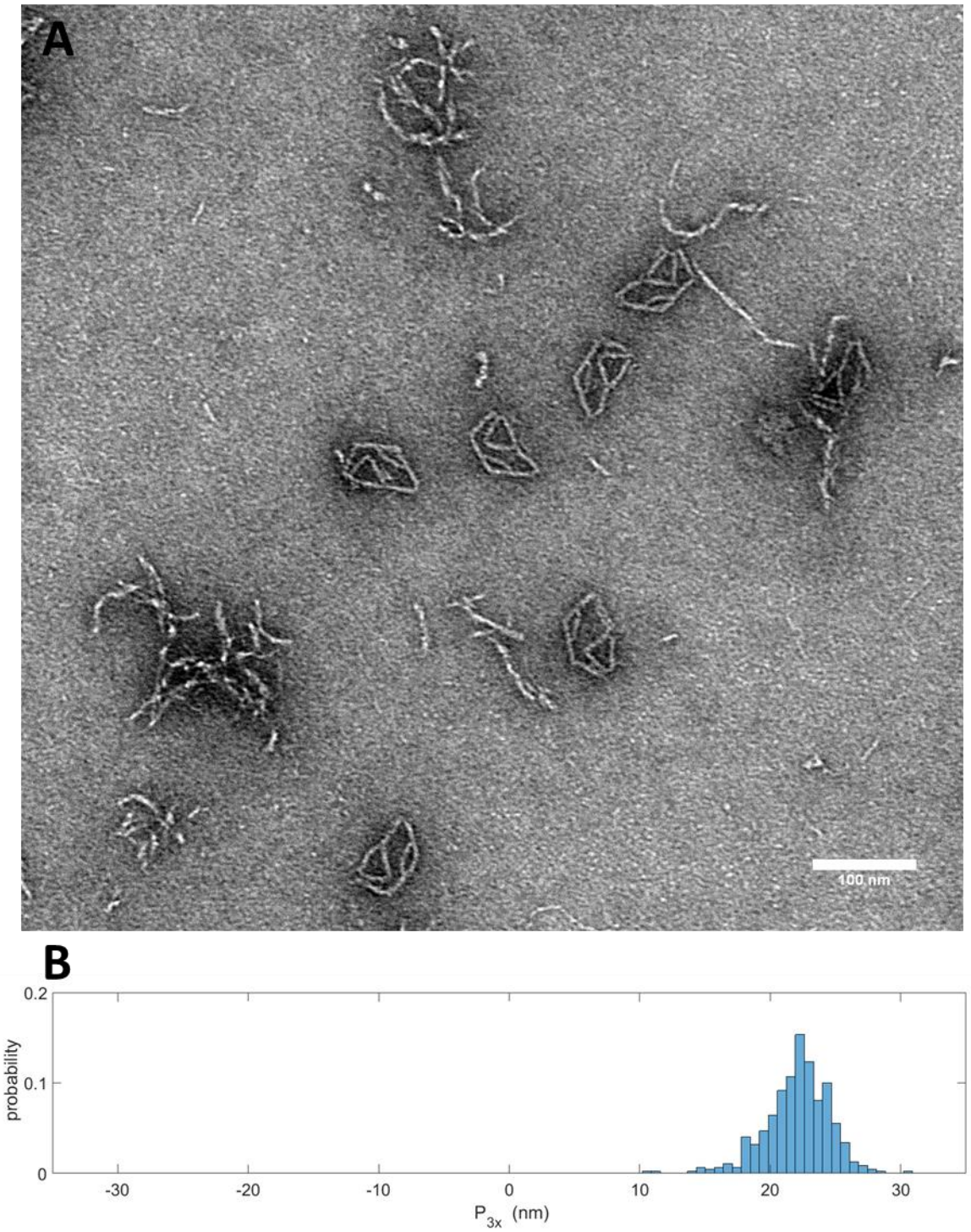

Figure S36: (A) TEM image of the SLL actuated to the right as the marker side, after agarose gel electrophoresis purification in 10mM $MgCl_2$ buffer. (B) Horizontal distribution of the tip.

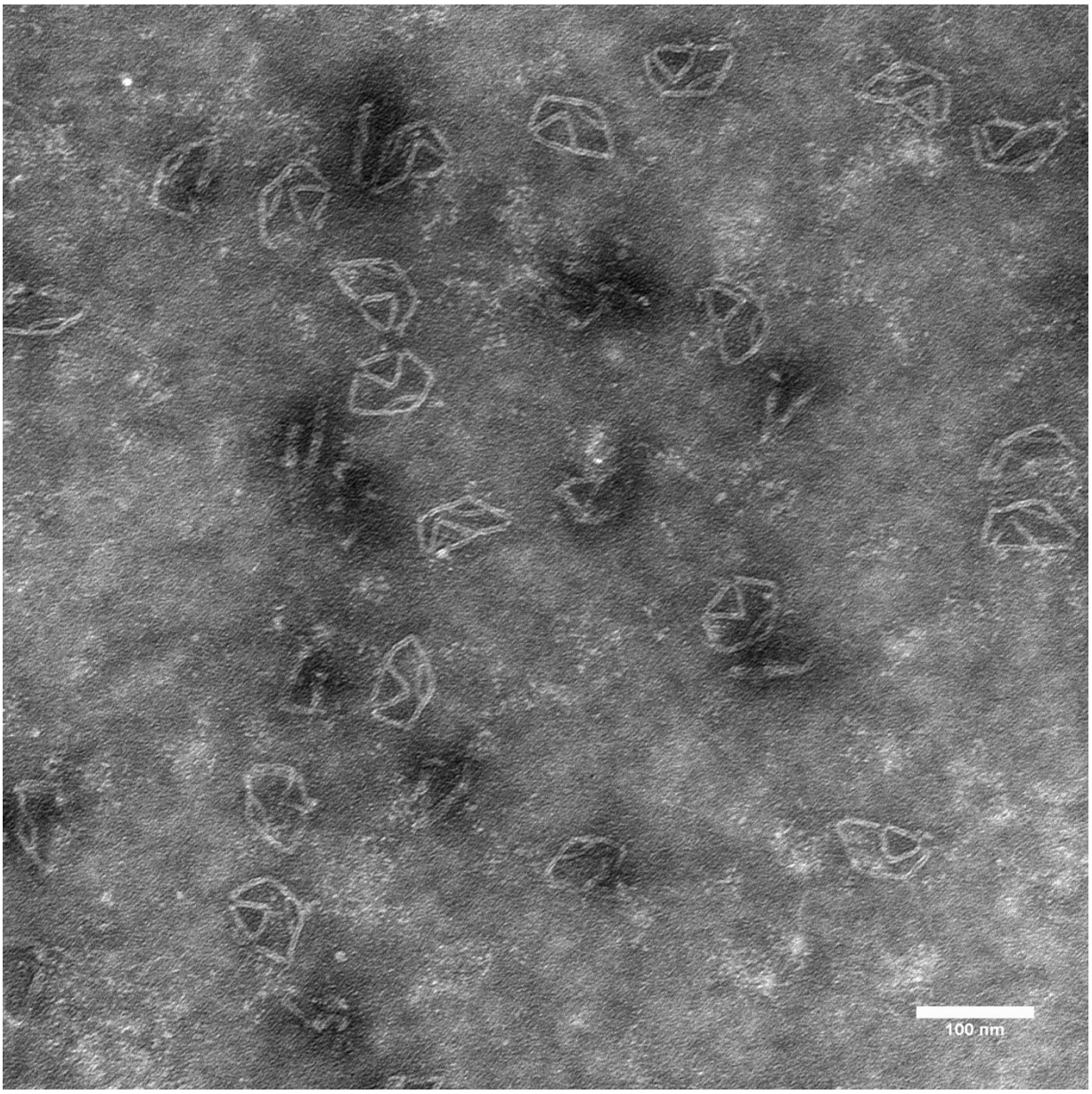

Figure S37: TEM images of the SLL after agarose gel electrophoresis purification in 5mM $MgCl_2$ buffer.

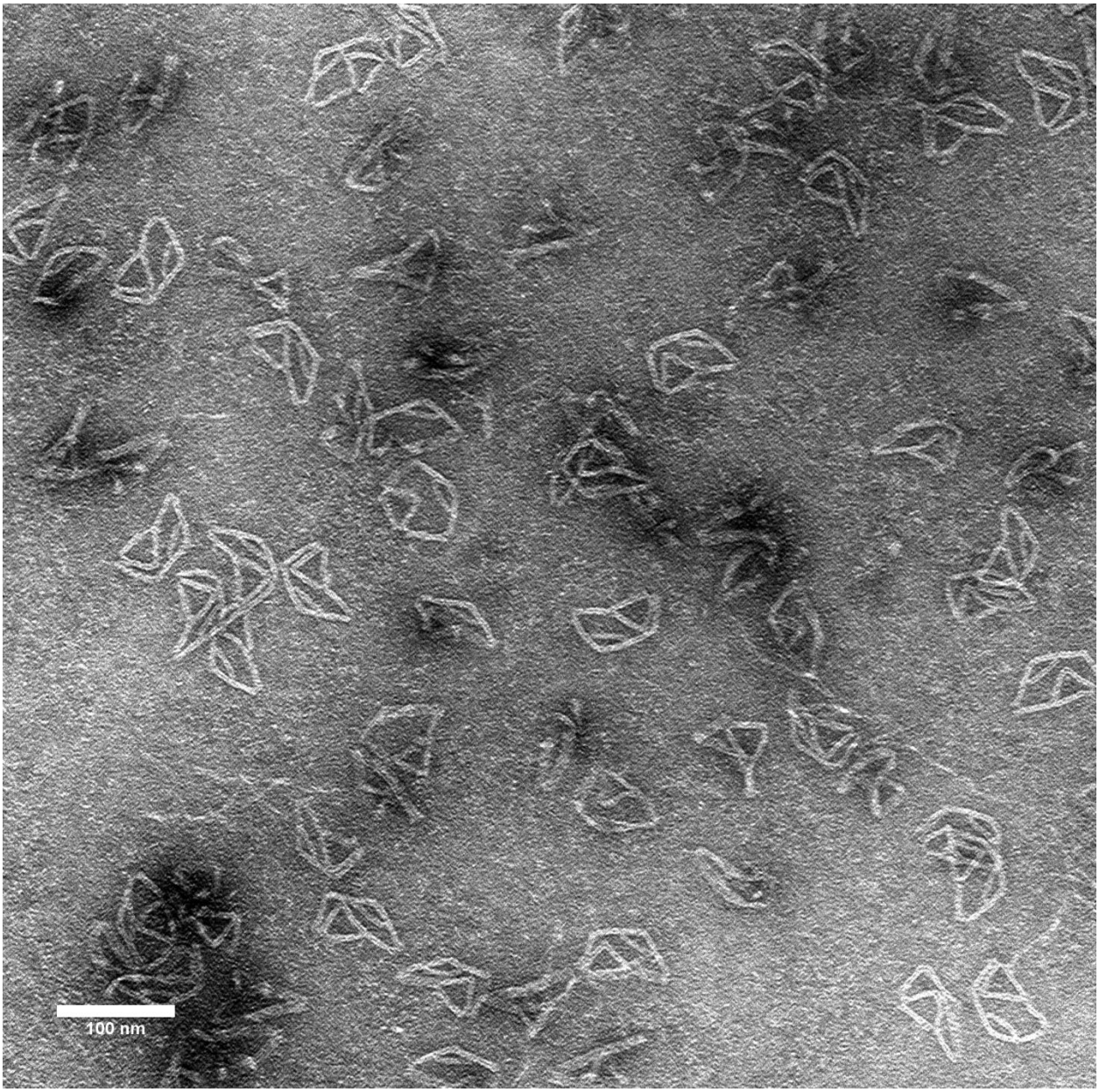

Figure S38: TEM image of the SLL after agarose gel electrophoresis purification in 20mM $MgCl_2$ buffer.

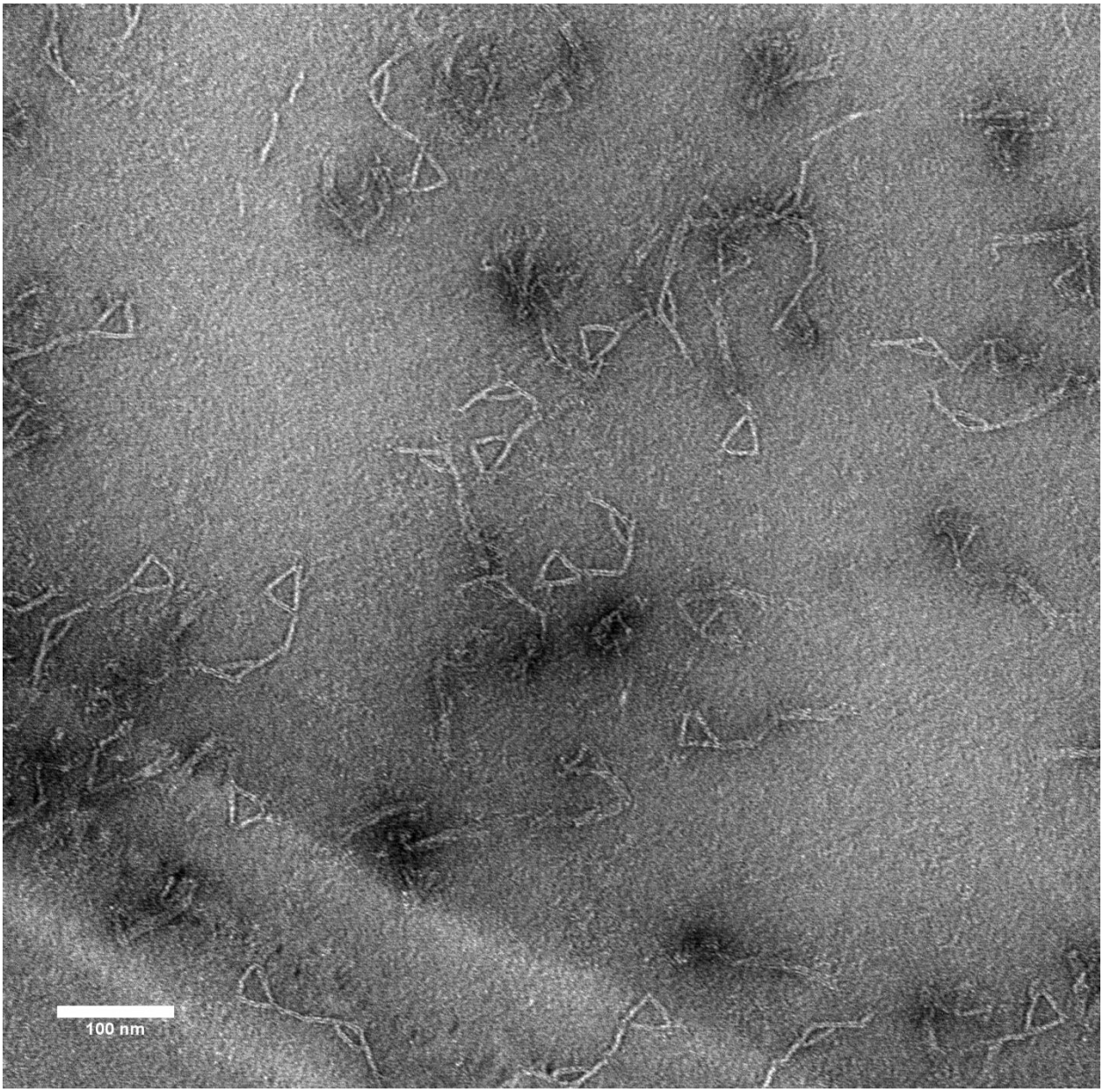

Figure S39: TEM image of the open-chain SLL after agarose gel electrophoresis purification in 10mM $MgCl_2$ buffer.

7. Staple sequences

Sequence	Length	Note as links
TGCCCCCTGCCTGTATTAAGTTCAATTACCTGAGCAAAAGAAGATCC	47	Link-6-16
ATTACCAATCAAGGAATCATAATTACTACAGAATCATGGT	40	Link-6-15
GACGAGAATTTCATCGGCATTTTCGGTCATAGCCC	35	Link-6-14
ATTAACTGAACATTTGCCAGAGGGGGTAATAGTA	34	Link-6-13
AAGAACCTATTAAGGCGTTATAGCGCGTACACC	33	Link-6-12
TGAGAAGTTTGCCTTTAGCGTCAGACTGAATA	32	Link-6-11
AAAGCTTCTGACCTAAATTTAATGGTTTGAA	31	Link-6-10
TGAGATAACCCTCGTTTACCAGACGACGATA	31	Link-6-09
CGCTCAAAATAGCGAGAGGCTTTTGCAAAA	30	Link-6-08
AGAAGACCGTGTGATAAATATTCTGAAACA	30	Link-6-07
CTGCTCATTCAGTGAATAAGGCTTGCCCT	29	Link-6-06
GCGAATTATTCATAGGCTGAGACTCCT	27	Link-6-05
CATCCTAATTTACGAGCAGAAT	22	Link-6-04
GCACCGTAATCAGTAGCGAGAA	22	Link-6-03
CAACACTATCTTAAGCCCAAT	21	Link-6-02
TTAATTTCATCCTGTTTAGTA	21	Link-6-01
TACCTTTTGCTTTAAAAAATGAAAATAGCAGCCTTTACAGAATC	44	Link-5-16
TGACAAGACCAGGCGGGCCTTGAGTTATTTTCATCGTAGGAGAG	44	Link-5-15
ATAGGCTGTATAAGTAGTGTACTGCAATAGCAAGCAAATCAACG	44	Link-5-14
TCGCCTGAGTCATAAAACATAAAAACAGGGAAGCGCATTAACA	43	Link-5-13
GCTCAGTAACCGGATTTTCATAATCAAAATCACCGGAACGGGT	43	Link-5-12
GCGGAATCTTGCTTTAGCCGTTTTAACAGTGCCCGTATTGCC	42	Link-5-11
CTCAAATACATCGGGCCGCGCCGTAATAAGTTTTAACGCAGA	42	Link-5-10
GGGTTGAGCTGACCTCCACCGGAACCGCCTCCCTCAGAATAC	42	Link-5-09
AGAAGGATTAGGATTAGCAGTTACAAAATCGCGCAGA	37	Link-5-08
ATCTATTCATTACCCAAATCAACGTAACAAA	31	Link-5-07
ATGGCTTTTGATGGCCGCCACCCTCAG	27	Link-5-06
CAGATGAATATACAATAGGTGTATCAC	27	Link-5-05
CGATTTTTTGTTTAGATATAGAAGGCT	27	Link-5-04
TCAACAGTTCAGAAAACGAGAATGAC	26	Link-5-03
ATTAGCGTTAAACAGTTA	18	Link-5-02
CTCATCGAGAGACGGGAG	18	Link-5-01
TTGGGAAGAACGCGAGTTTTTAACAAATCATAGGTCTGAGGAAACATAGCGATAGC	56	Link-4-16
TTGTATCGAAACAGCGTTGTACCAAAAACATTATATAACTATATGTAAATGAAT	54	Link-4-15
AATTTCTTGTTTATCACCTGTAATACTTATCCAATAAATCTAA	43	Link-4-14
GCGCGAGCTGTTTAGCTTCAACGCAAGGATAAAAATTTTGTAG	43	Link-4-13
CAATAACCTGAAAAGAACTTGCGGGAGAAGCCTTAGTCA	39	Link-4-12

TTGCTTCTAGAATCCTTGAAATTACGAGGCATAGTAAG	38	Link-4-11
ATCGTTGATACCGATAGTTGCGCCGACAATG	31	Link-4-10
CAGGCAAAAGGAAATTCTACAGATTCAAAAG	31	Link-4-09
ATAACGCCAAAAGATTTAGGAATACCA	27	Link-4-08
AATATATGTGAGTTTCAAATATATTTT	27	Link-4-07
TTCATCAGTTGAGAACTAACGGAACAA	27	Link-4-06
AAGCCTCAGAGCATAAAGCATA	22	Link-4-05
GTGTAGGTAATAATAGTATAGA	22	Link-4-04
AAAAAGGCTCCAAGGCAAAGA	21	Link-4-03
ACCATTAGATTCATATATTTT	21	Link-4-02
TTCCCTTGTAAATCGTTT	18	Link-4-01
AGAAAAGTAAGCAGATAGGGCAGAGGCATGAATCTTACCAACTGAAATAGCAATAGCTA	59	Link-3-26
CGCAAAGACACCACGGAATAAGTTTATTTCAAAAGGGCGACAAAAATACATACATAAAG	59	Link-3-25
ATTAAAGGTGAATTATCACCGTCACAAATAGTTCAACCGATTGAGGGAGGGAAGGTA	57	Link-3-24
CGCTCAACCACCATTATAGAGCCAGCAAAATCCCAGAGCCAAATGAGAA	49	Link-3-23
CAGAATGGGCCGCCAGCCACCAGAACCACCAACCAGTAGAGTAGGG	46	Link-3-22
TAATACCAGTATCAACAATAGATAAGTCCAAGCTAACGAGCGTC	44	Link-3-21
CTTAATGCGTGTTCAGCTAATGCAGTGCCAGTTGCACCCAG	41	Link-3-20
TTTCCAGAGCCTAATTAACGCGCCCAGTAATAATTTAACA	40	Link-3-19
AACAGCCATATTATTACGACAATAGGTAAAGATTAAAGC	39	Link-3-18
TCGCCATAGAGAATATAAAGTACGCTATTTTACAAAATA	39	Link-3-17
GAAACGTCAAATTCTTTTACCGAACAAAGTTACCAGAA	38	Link-3-16
CTACAATTTTATCCTTTTCGAGCTGTTTATAAAGCCAA	38	Link-3-15
AATAACGGAATACCCACGACTTGAGCCATCATG	33	Link-3-14
TCCAAAATCCTCTAATTCTGCGCGAGGCGTT	31	Link-3-13
AGCCGCATTGACAGGAGGTTGAGGCAGGTCA	31	Link-3-12
CCAATGAAGCCTTAAATCAAGATTAGTTCGA	31	Link-3-11
CAAAAAACAACACAGTCTCTGAATTTATCAG	31	Link-3-10
ACGCCAATTGGGAATCCATTAGCAAGGCCG	30	Link-3-09
ATATGCGTTATACACCAATGAAACCAT	27	Link-3-08
ATGTTAGCAAACGGAACTGGCATGATT	27	Link-3-07
TAAGAGCAAGAAACTGAACAAGAAAAA	27	Link-3-06
CAGCGCCAAAGATGTCACAATCAAT	25	Link-3-05
CCCTCAGAGCCACCACCCCCGT	22	Link-3-04
ATTCTAAGAATCCAGACGTATC	22	Link-3-03
ACAAACAAATGTAAGCGTCAT	21	Link-3-02
CGGGAGGTTTTCCAAATAAGA	21	Link-3-01
ATTAGAGCCGTCAATAGACAACTCCATTTTCAATCGCCAT	40	Link-2-17
AATCCTTTCGGAACAAGGAAGCCCGAAAGACTTCAAAT	38	Link-2-16
CCATAGAGCCTTGCTGAACCTCATGAGGAAGGCGCA	36	Link-2-15
TCAACAGTTGAAAGGAATAATATCAAGTTTAGTA	34	Link-2-14

CTGAATAATGGAAGGGTTCAATTCATATCAGGTC	34	Link-2-13
AAATATCTTTAGGAGCAAAATCTATCAGAACC	32	Link-2-12
TTTGTATCATCGCCTGATAAATTGTGTCGACC	32	Link-2-11
CCGCCACCCTCAGAACGAACGAGGTTATCTA	31	Link-2-10
TAAAAATACCGAACGAAACAGTGCCACGTTA	31	Link-2-09
ATCAAGCAAAGCGGATTGCATCAAAAAGAT	30	Link-2-08
GCCACCCTCAGAGCCAAATCCGCCTAATAG	30	Link-2-07
TTTACCCTGACTATTAGGTTCAAAATTA	28	Link-2-06
CATTATCATTTTGGCCCGAACGTTATT	27	Link-2-05
ATAGCCCTAAAACGGGATAGCAAGCCC	27	Link-2-04
TTACAAACAATTCGATAATACATTTGA	27	Link-2-03
TAAATCAAAACAATATAATCC	21	Link-2-02
TACTCAGGAGACCCTCAATCA	21	Link-2-01
GTTTAGACTGGATAGCGTCCAATACT	26	JointB- Up(L5)-S-08
AACGGTGTACAGACCAGGCGC	21	JointB- Up(L5)-S-07
GCCATCATCAAGAGTAATCT	20	JointB- Up(L5)-S-06
ATTAAGAAACAACGTCGAGA	20	JointB- Up(L5)-S-05
AGGATAGCCCGGAGTAACAG	20	JointB- Up(L5)-S-04
AGCAGAATACCAGGGGTTTT	20	JointB- Up(L5)-S-03
AATATATTCATTGAATCCCC	20	JointB- Up(L5)-S-02
CAGTATAAGTGCTAACGGAT	20	JointB- Up(L5)-S-01
GTTTAGACTGGATAGCGTCCAATACTCAGTTTATTTTC	38	JointB- Up(L5)-08
AACGGTGTACAGACCAGGCGCCAGTTTATTTTC	33	JointB- Up(L5)-07
GCCATCATCAAGAGTAATCTCAGTTTATTTTC	32	JointB- Up(L5)-06
ATTAAGAAACAACGTCGAGACAGTTTATTTTC	32	JointB- Up(L5)-05
AGGATAGCCCGGAGTAACAGCAGTTTATTTTC	32	JointB- Up(L5)-04
AGCAGAATACCAGGGGTTTTCAGTTTATTTTC	32	JointB- Up(L5)-03
AATATATTCATTGAATCCCCCAGTTTATTTTC	32	JointB- Up(L5)-02
CAGTATAAGTGCTAACGGATCAGTTTATTTTC	32	JointB- Up(L5)-01
ATCACTCCGGCTTAGGTTGGGTTATGACGCTTGCTTCATTTGGG	44	JointA-Up(L4)-S-08
CTACGTTAATAAAACGAGACTACCAAAACTTTGAATAACC	40	JointA-Up(L4)-S-07
TTAGATTAAGACGCTGAGAAGTATTATATTTTAATTAATT	40	JointA-Up(L4)-S-06
GACAAAGAAACTGATGCAAATCCTCGAGGTG	31	JointA-Up(L4)-S-05
ATAGTGAATCGCTATTAATCGCAA	24	JointA-Up(L4)-S-04
CTCATTATACCAGTCAGGACG	21	JointA-Up(L4)-S-03
CATTGTGGCATCGCCTTTAA	20	JointA-Up(L4)-S-02
ACCCACATTTCGCAAATGGT	20	JointA-Up(L4)-S-01
ATCACTCCGGCTTAGGTTGGGTTATGACGCTTGCTTCATTTGGGACTTTATACCCC	56	JointA-Up(L4)-08
CTACGTTAATAAAACGAGACTACCAAAACTTTGAATAACCACTTTATACCCC	52	JointA-Up(L4)-07
TTAGATTAAGACGCTGAGAAGTATTATATTTTAATTAATTACTTTATACCCC	52	JointA-Up(L4)-06
GACAAAGAAACTGATGCAAATCCTCGAGGTGACTTTATACCCC	43	JointA-Up(L4)-05

ATAGTGAATCGCTATTAATCGCAAACTTTATACCCC	36	JointA-Up(L4)-04
CTCATTATACCAGTCAGGACGACTTTATACCCC	33	JointA-Up(L4)-03
CATTGTGGCATCGCCTTTAAACTTTATACCCC	32	JointA-Up(L4)-02
ACCCACATTTCGCAAATGGTACTTTATACCCC	32	JointA-Up(L4)-01
ACCCTGTACTGAGAGCCAGCAGCAAATGAACTAACAAGACCT	42	Joint B- Bottom(L2)-S-08
TAAGAAGAAACCACCAGAAGGAGCGGAATCCGCCTGCACCAC	42	Joint B- Bottom(L2)-S-07
TCAGATATTCCTGATTATCAGATGATGGAGAACCTA	36	Joint B- Bottom(L2)-S-06
CACCCAAGCATCAGCGGTCAGTATTAACATATC	33	Joint B- Bottom(L2)-S-05
CAGCAGAAGATAAAACAGATAG	22	Joint B- Bottom(L2)-S-04
GACGGTCAATCATAAGGGAACC	22	Joint B- Bottom(L2)-S-03
TTTGCACGTAAAACAGAAATAA	22	Joint B- Bottom(L2)-S-02
GCTCCATGTTACTTAGCCGCGC	22	Joint B- Bottom(L2)-S-01
ACTACAAAATCGACCCTGTACTGAGAGCCAGCAGCAAATGAACTAACAAGACCT	54	Joint B- Bottom(L2)-08
ACTACAAAATCGTAAGAAGAAACCACCAGAAGGAGCGGAATCCGCCTGCACCAC	54	Joint B- Bottom(L2)-07
ACTACAAAATCGTCAGATATTCCTGATTATCAGATGATGGAGAACCTA	48	Joint B- Bottom(L2)-06
ACTACAAAATCGCACCCAAGCATCAGCGGTCAGTATTAACATATC	45	Joint B- Bottom(L2)-05
ACTACAAAATCGCAGCAGAAGATAAAACAGATAG	34	Joint B- Bottom(L2)-04
ACTACAAAATCGGACGGTCAATCATAAGGGAACC	34	Joint B- Bottom(L2)-03
ACTACAAAATCGTTTGCACGTAAAACAGAAATAA	34	Joint B- Bottom(L2)-02
ACTACAAAATCGGCTCCATGTTACTTAGCCGCGC	34	Joint B- Bottom(L2)-01
GAAGTCCCTGAACAAAGTCAGAGGGTAATCTTATCATTGATG	42	Joint A -Bottom(L6)-S-08
AAAACAATATCAGAGAGATAACCCACAATGTAGAAAATTAC	41	Joint A -Bottom(L6)-S-07
ATACCTAAACACCTAATCGGCTGTCTTTCTGAG	33	Joint A -Bottom(L6)-S-06
TGAAAATTTCGGAACGGGTATTAAACCAAGTAC	33	Joint A -Bottom(L6)-S-05
TTAATTTCAACTTTAATCATTG	22	Joint A -Bottom(L6)-S-04
AGAACGAGTAGTAAATTGGGCT	22	Joint A -Bottom(L6)-S-03
ATTTAACAATTTCATTTGAATT	22	Joint A -Bottom(L6)-S-02
AAACAAACATCAAGAAAACAAA	22	Joint A -Bottom(L6)-S-01
TTCCTTATTATTGAAGTCCCTGAACAAAGTCAGAGGGTAATCTTATCATTGATG	54	Joint A -Bottom(L6)-08
TTCCTTATTATTAAAACAATATCAGAGAGATAACCCACAATGTAGAAAATTAC	53	Joint A -Bottom(L6)-07
TTCCTTATTATTATACCTAAACACCTAATCGGCTGTCTTTCTGAG	45	Joint A -Bottom(L6)-06
TTCCTTATTATTTGAAAATTTCGGAACGGGTATTAAACCAAGTAC	45	Joint A -Bottom(L6)-05
TTCCTTATTATTTTAATTTCAACTTTAATCATTG	34	Joint A -Bottom(L6)-04
TTCCTTATTATTAGAACGAGTAGTAAATTGGGCT	34	Joint A -Bottom(L6)-03

TTCCTTATTATTATTTAACAATTTCATTTGAATT	34	Joint A -Bottom(L6)-02
TTCCTTATTATTAAACAAACATCAAGAAAACAAA	34	Joint A -Bottom(L6)-01
CTGTAGCCGGAAGTTAGCTGATTGCCCTTCACCGCCTGGAAGAGAATTCAA	51	GroundLink-3-16
GTAAAACTCGGGCAACTCCATTAAACGGGTAAAATACGTAATGCCA	46	GroundLink-3-15
TAATTGCTCCTTTTGATAAGAGGTCATTTAAGTGTTTTGGCCTTC	45	GroundLink-3-14
GAGCAAACCCCTGAGATGAGGACTAAAGACTTTTTCATGAAGCT	44	GroundLink-3-13
ATTCAACAGGAGGCCGATTAAAGGGATTTAATGCTAGAGTCTG	43	GroundLink-3-12
CATTGAACGGTACGCCAGAATCCTGAGTTGCGGATGGTAATC	42	GroundLink-3-11
TTCACGATGAACGGCTTAGAGCTTAATTGCTGAATATTAG	40	GroundLink-3-10
GCTTGAGTTGCAGCAAGCGGTCCACGCATCAGGTCTCGG	39	GroundLink-3-09
ATCGGAACGAGGGTAGCAACGGCTACACAACCCGATTG	38	GroundLink-3-08
TGTCTTCGCGTCTTATAATCAGTGAGGCCACCGA	34	GroundLink-3-07
CCTGGTAGCTCAACATGTTTTAAATATGCAA	31	GroundLink-3-06
CCATCAAAAATAAAATCATATGTACCC	27	GroundLink-3-05
TTTTTCTTTTCACCAGTGAGAAGCA	25	GroundLink-3-04
ACAGAAATGTGAGCGAGTAAGAG	23	GroundLink-3-03
TACAAAGGCTTGGTTTGCCCC	21	GroundLink-3-02
GCGGGAGCTATCCGTGGGAAC	21	GroundLink-3-01
TATTAAAGAACGTGGACTCCAACGTCAAAGCCAGTGCTATGGGATTTGGTGTA	53	GroundLink-2-27
AGCGCCATGGCCTTGCTGAGTAGAAGAACTCATGCTTTCCATGGGATACAGG	52	GroundLink-2-26
TAGAACGAGCACGTATAACGAACTATCTCGCCATTGGTCACGTTTGCTAA	50	GroundLink-2-25
CAAGAAGGAATTATTAATGCCGGAGAGGCATTCCATGCCGCTAC	44	GroundLink-2-24
ACAACTTTCTGTTTGAAACCGTCTATCATCACCCAAATCAGTTT	44	GroundLink-2-23
TATTACGCCTTAATGCATAACAGTTGATTCCCAATTCTGCCGTT	44	GroundLink-2-22
TAGAAAGGGTCACCCTTGGGGTCGAGGTGCCGTAAAGCACGCTG	44	GroundLink-2-21
AGTTAGTCACGAGCAACTGTTGGGAAGGTTGCTTTGTAAAGTAC	44	GroundLink-2-20
ACGCCAGGAGTTTTTCAGCAGCGAAAGCAGGCGAAAATCCAAC	43	GroundLink-2-19
TAATTTTTGCAGGGAGAACCCTAAAGGGAGCCCCCGATTTAG	42	GroundLink-2-18
CCGCTTTTGCGGGATCAACAACTAGCGATTAACTCTTCGC	40	GroundLink-2-17
TCCGAAATCGGCAAAAATTTTCTGCAAGCTTGCCAGGCAA	40	GroundLink-2-16
GGTGTCTGGAAGTTTGTAGCTATGTGCGGGCGTTGGGTA	39	GroundLink-2-15
ACCACACCCGCCGCGCAGCTGGCCTGATAAGCGAATAA	38	GroundLink-2-14
GATGGGCGCACTTGCCTGGTAATATCCAGAACAATATT	38	GroundLink-2-13
AGGGCGCGTACTATGGGCGATCGTTTTGAGAGTGAGAA	38	GroundLink-2-12
TATTCGGTCGCTGAGGCTTTCACGTTGAGAAAGGA	35	GroundLink-2-11
CATCAATATGATATTCAACGAACGAGTGCGTAACC	35	GroundLink-2-10
CTGCCGTTGTAAAACGACGGGGCGAAATGGTGGT	34	GroundLink-2-09
TCCCTCAGCGGAGATCGGATTGACCGTATCGT	32	GroundLink-2-08
AGGGAAGGGGGATGTTAAATCGGTTAAAGG	30	GroundLink-2-07
CTAGGAAAGAAAGCGAAAGGAGCGGGCGCT	30	GroundLink-2-06
CTGGTGCCGGAAACATGCCTGCAGGTC	27	GroundLink-2-05

GGTCACGCTGCAGATTTAGTT	21	GroundLink-2-04
CGAACGTGGCGAAAATCTCCA	21	GroundLink-2-03
AATAACATCATCGTAAC	17	GroundLink-2-02
GTAAATGATCCCTTATA	17	GroundLink-2-01
GGCGCTCATAGTTCATAGCTAATCAGCTGCCTCAGGTACCTACATCACGCAA	52	GroundLink-1-28
TGTGAAATTGCATTAAGGCACCAACCTAAAACGAAAGAGCTACAACGGCTCA	52	GroundLink-1-27
CCAGCCATTGCAACAGGAAAAACGCTCATGGAAAAAGATCGCACGA	46	GroundLink-1-26
CGACGATCTAAAGTTTTGTCCGAGATAGGGTTCGGTTTGCGTATTG	46	GroundLink-1-25
TAACAGCATAAATAAGAATAATATTTAACACGACCAAAGCGAAC	44	GroundLink-1-24
AACATACCGCTTTCCATACACTAAAACACTCATCTTTGACCG	42	GroundLink-1-23
AATTCGTAGGGAGTGTTGTTCCAGTTTGGAACAAGAGTCCA	41	GroundLink-1-22
ATTAACCGTTGTAGCATTGAGGGGACTCCAGCCGAGCTCG	40	GroundLink-1-21
CAGACCGGAAGCAAACAAACAGGACGTTAATATTCCACAC	40	GroundLink-1-20
TAGAGAGTACCTGAGAACCAATATTTTGTTAGTTTCCTG	39	GroundLink-1-19
CTAGAGGATCCCCGGGTACCAGCTTTCCGGCACCGCT	37	GroundLink-1-18
CAATTTTGTTAAAATTCGCGGATTATTGTCAGGAT	35	GroundLink-1-17
CTCACATTAATTGCGTTGCGCTCACTGCCGAGC	33	GroundLink-1-16
AAGAAGTCGGGAAACCTGTCGTGCCAGCTGTT	32	GroundLink-1-15
GGTGATGAATCGGCCAACGCGCGGGGAGAATC	32	GroundLink-1-14
CGGAACTGAGTTATAAGCAACGTGGCACGAGC	32	GroundLink-1-13
ATGGTAGCGTAACAGTATCGCATTTTTTTCTG	32	GroundLink-1-12
ATCCCCTGTAGCATCAGAAAAGCCCCAATCCA	32	GroundLink-1-11
TCCATTTTGACGCTCAATCGTCTGAAATATT	31	GroundLink-1-10
ACAGTACATTGGCAGATTCACCAGTCAATTG	31	GroundLink-1-09
TAAAAGATTGTTCGTCACCAGTACAAAGCAA	31	GroundLink-1-08
AAATGGTTGATAATTCCACAGACAGCCCCAG	31	GroundLink-1-07
GTGCATCTGCCAGTATACTTCTTTGATT	28	GroundLink-1-06
ATCAAAAGAATAGCCGTCTTTCCAGACG	28	GroundLink-1-05
TGACCTGAAAGCGGTGTAAAGCCTGGG	27	GroundLink-1-04
TAGGAACCCATGTACCCCCAGCGATTA	27	GroundLink-1-03
CGCGTTTTAATTCAGACAATATTTTTG	27	GroundLink-1-02
TTCAGTAATAAAAGGGACATTCTGGC	26	GroundLink-1-01
ATTTTAAGAACT	12	Dummy Connection-16
TTCAGGTTTAAC	12	Dummy Connection-15
AACAACCATCGC	12	Dummy Connection-14
AAAGAGGACAGA	12	Dummy Connection-13
ACTGACCAACTT	12	Dummy Connection-12
AAGTACAACGGA	12	Dummy Connection-11
ACAGTACATAAA	12	Dummy Connection-10
TGGCTATTAGTC	12	Dummy Connection-09

GACAGTCAAATC	12	Dummy Connection-08
TAATGCGCGAAC	12	Dummy Connection-07
ACGCATAACCGA	12	Dummy Connection-06
TGAGAAAGGCCG	12	Dummy Connection-05
CTTTTTTAATGG	12	Dummy Connection-04
AAATTGCGTAGA	12	Dummy Connection-03
CCAAGCGCGAAA	12	Dummy Connection-02
AATTACCTTATG	12	Dummy Connection-01
CGATTTTGTAGTGAAAATAAACTG	24	ClosingStrandB
AATAATAAGGAAGGGGTATAAAGT	24	ClosingStrandA

Reference:

(1) Douglas, S. M.; Marblestone, A. H.; Teerapittayanon, S.; Vazquez, A.; Church, G. M.; Shih, W. M. Rapid Prototyping of 3D DNA-Origami Shapes with caDNAno. *Nucleic Acids Res.* **2009**, *37* (15), 5001–5006.

(2) Castro, C. E.; Kilchherr, F.; Kim, D.-N.; Shiao, E. L.; Wauer, T.; Wortmann, P.; Bathe, M.; Dietz, H. A Primer to Scaffolded DNA Origami. *Nat. Methods* **2011**, *8* (3), 221–229.

(3) Kim, D.-N.; Kilchherr, F.; Dietz, H.; Bathe, M. Quantitative Prediction of 3D Solution Shape and Flexibility of Nucleic Acid Nanostructures. *Nucleic Acids Res.* **2012**, *40* (7), 2862–2868.

(4) Doye, J. P. K.; Ouldridge, T. E.; Louis, A. A.; Romano, F.; Šulc, P.; Matek, C.; Snodin, B. E. K.; Rovigatti, L.; Schreck, J. S.; Harrison, R. M.; et al. Coarse-Graining DNA for Simulations of DNA Nanotechnology. *Phys. Chem. Chem. Phys.* **2013**, *15* (47), 20395–20414.

(5) Snodin, B. E.; Randisi, F.; Mosayebi, M.; Šulc, P.; Schreck, J. S.; Romano, F.; Ouldridge, T. E.; Tsukanov, R.; Nir, E.; Louis, A. A. Introducing Improved Structural Properties and Salt Dependence into a Coarse-Grained Model of DNA. *J. Chem. Phys.* **2015**, *142* (23), 06B613_1.

(6) E. Castro, C.; Su, H.-J.; E. Marras, A.; Zhou, L.; Johnson, J. Mechanical Design of DNA Nanostructures. *Nanoscale* **2015**, *7* (14), 5913–5921.

(7) Zhou, L.; Marras, A. E.; Su, H.-J.; Castro, C. E. Direct Design of an Energy Landscape with Bistable DNA Origami Mechanisms. *Nano Lett.* **2015**, *15* (3), 1815–1821.

(8) Thirumalai, D.; Ha, B.-Y. Statistical Mechanics of Semiflexible Chains: A Meanfield Variational Approach. *ArXivcond-Mat9705200* **1997**.

(9) Waldron, K. J.; Kinzel, G. L.; Agrawal, S. K. *Kinematics, Dynamics, and Design of Machinery*; John Wiley & Sons, 2016.

(10) Li, X.; Ding, X.; Chirikjian, G. S. Analysis of Angular-Error Uncertainty in Planar Multiple-Loop Structures with Joint Clearances. *Mech. Mach. Theory* **2015**, *91*, 69–85.
(11) Marras, A. E.; Zhou, L.; Su, H.-J.; Castro, C. E. Programmable Motion of DNA Origami Mechanisms. *Proc. Natl. Acad. Sci.* **2015**, *112* (3), 713–718.
(12) Sharma, R.; Schreck, J. S.; Romano, F.; Louis, A. A.; Doye, J. P. K. Characterizing the Motion of Jointed DNA Nanostructures Using a Coarse-Grained Model. *ACS Nano* **2017**.
(13) NUPACK: Analysis and design of nucleic acid systems - Zadeh - 2011 - Journal of Computational Chemistry - Wiley Online Library https://onlinelibrary.wiley.com/doi/full/10.1002/jcc.21596 (accessed Apr 6, 2018).